ISSN: 2376-2136 (Print)
ISSN: 2376-2144 (Online)

Trends in Renewable Energy

Volume 2, Issue 3, December 2016
Special Issue on Smart Grid (1)

futureenergysp.com
thefutureenergy.org

Trends in Renewable Energy

ISSN: 2376-2136 (Print) ISSN: 2376-2144 (Online)

http://futureenergysp.com/

Trends in Renewable Energy is an open accessed, peer-reviewed semi-annual journal publishing reviews and research papers in the field of renewable energy technology and science.

The aim of this journal is to provide a communication platform that is run exclusively by scientists working in the renewable energy field. Scope of the journal covers: Biofuel, Bioenergy, Biomass, Biorefinery, Biological waste treatment, Bioprocessing, Catalysis for energy generation, Energy conservation, Energy delivery, Energy resources, Energy transformation, Energy storage, Environmental impact, Feedstock utilization, Future energy development, Green chemistry, Green energy, Microbial products, Physico-chemical process for Biomass, Policy, Pollution, Renewable energy, Thermo-chemical processes for biomass, etc.

The Trends in Renewable Energy publishes the following article types: peer-reviewed reviews, mini-reviews, technical notes, short-form research papers, and original research papers.

The article processing charge (APC), also known as a publication fee, is fully waived for the Trends in Renewable Energy.

Editorial Team of Trends in Renewable Energy

EDITORIAL BOARD

Table of Contents

Volume 2, Issue No. 3, December 2016

Special Issue on Smart Grid (1)

Trends in Renewable Energy
OPEN ACCESS ISSN: 2376-2144
EDITORIAL futureenergysp.com/index.php/tre

Green Technology and Sustainable Development of Renewable Energy

Dr. Suzana Yusup * (Associate Professor, Chemical Engineering Department, Universiti Teknologi PETRONAS, Malaysia)

31750, Tronoh. Perak., Malaysia
Tel. No.: +605-3688217 Fax No. +605-3688204

Received July 12, 2016; Published July 15, 2016

Carbon dioxide (CO_2) and other greenhouse gases (GHG) emissions, which cause global warming, have become a major worldwide concern with ten global 'mega' challenges that are currently impacting the planet in particular climate change, water, energy, and material resource scarcity. Increase in urbanization rate will continue to increase its need for natural resources, building materials, power and electricity, water, etc. that leads to bio-capacity deficit with a sharp increase in generation of ecological footprints. Power-generating plants running on fossil fuels have been identified as the main source of greenhouse gases (GHG). Approximately, 80% of the world primary energy consumption is still dependent on fossil fuels; thus, the substitution by renewable energy sources, in conjunction with other clean energy sources, appears to be the best and necessary alternative. There are many other sources of renewable energy such as solar, wind, and geothermal, but biomass have been receiving a lot of attention lately. Biomass has gained increased attention in the past decade because it does not only provide an effective option for the provision of energy services from a technical point of view, but also based on resources that can be utilized on a sustainable basis all around the globe. Another benefit of biomass utilization is that this resource can be converted to C3-C4 hydrocarbons and/or synthetic gas (H_2 and CO).

Statistics shows that the urban areas with industrial, residential and commercial activities are the large energy "deficit zones". Thus, the transfer of biomass energy sources from the "surplus zones", which are those surrounding rural / plantation areas to the major urban cities, can be a solution that bring numerous benefits to the regions: (i) Environmental – minimization of CO_2 emissions and other gases of the greenhouse effect (ii) Energy - improvement in the regional energy balance, reinforcement of energy independence, and (iii) Economical – maximization of the utilization of local energy sources and adding the value to the "waste".

There is a great potential for exploitation of local energy sources from wastes but the strength of policy support and stimulation measures are far from sufficient. At this moment, there is lack of studies about the integration of different types of wastes and the application of green technology approach, in addition to proper supply chain analysis and synthesis for waste-to-energy (WTE) system. These missing studies are crucial for solving both energy and environmental problems especially in the urban area. Further innovative and cost effective process needs to be developed to ensure the competitiveness of green industry. Producing biodiesel from non-edible feedstock is one of the solutions to reduce the import volume. Furthermore, public awareness and acceptance on the

**Corresponding author:* drsuzana_yusuf@petronas.com.my

Tr Ren Energy, 2016, Vol.2, No.3, 83-84. doi:10.17737/tre.2016.2.3.0024

utilization of green fuels needs to be promoted and increased. Knowledge dissemination on the advantages of the biofuel utilization in the transportation sectors could be achieved through outreach initiatives to young minds and public.

Increasing demand of transportation fuel has made utilizing biofuels more attractive since it helps to reduce CO_2 to 78.45% compared to if purely fossil fuel based is utilized. The sector which emits the most CO_2 is the transportation sector. Energy for transportation is projected to be the fastest growing sector during the next five years, expanding at an annual rate of 5.3%. Non-edible resources as fuel are thus important to avoid food vs fuel crisis and reduce dependency on fossil fuel. Furthermore, world population is projected to grow from 6.5 billion in 2005 to nearly 9.2 billion by 2050. To feed a population of more than 9 billion, global food production must be doubled by 2050. Additionally, reliance on a single source of feedstock for biodiesel production has its setback. Thus, diversification of the feedstock towards non-edible materials with a minimal retrofit to existing production facilities will help to overcome the situation. Sustainable development of the energy sector is one of the key factors to maintain economic competitiveness and progress.

The initiative of the Green Technology promotes minimization growth of energy consumptions while enhancing economic development. In addition, it will increase national capability, capacity and awareness for innovation in Green Technology. Overall, the policies and incentives on renewable energy are important to promote low carbon economy and society in future.

Trends in Renewable Energy
OPEN ACCESS ISSN:2376-2144
Peer-Reviewed Article futureenergysp.com/index.php/tre

Measurement Differences, Faults and Instabilities in Intelligent Energy Systems – Part 1: Identification of Overhead High-Voltage Broadband over Power Lines Network Topologies by Applying Topology Identification Methodology (TIM)

Athanasios G. Lazaropoulos[1]

1: School of Electrical and Computer Engineering, National Technical University of Athens, 9 IroonPolytechniou Street, Zografou, GR 15780 Greece

Received August 25, 2016; Accepted September 23, 2016; Published October 3, 2016

This first paper considers the identification of the structure of overhead high-voltage broadband over power lines (OV HV BPL) network topologies by applying the best L1 Piecewise Monotonic data Approximation (best L1PMA) to measured OV HV BPL transfer functions. Even if measurement differences occur during the determination of an OV HV BPL transfer function, the corresponding OV HV BPL network topology may be revealed through the curve similarity of the best L1PMA result compared with the available records of the proposed OV HV BPL transfer function database.
The contribution of this paper is triple. First, based on the inherent piecewise monotonicity of OV HV BPL transfer functions, best L1PMA is first applied during the determination of theoretical and measured OV HV BPL transfer functions. Second, the creation procedure of the OV HV BPL network topology database is demonstrated as well as the curve similarity performance metric (CSPM). Third, the accuracy of the proposed Topology Identification Methodology (TIM) is examined in comparison with the traditional TIM with respect to the nature of the measurement differences during the determination of OV HV BPL transfer functions.

Keywords: Smart Grid; Intelligent Energy Systems; Broadband over Power Lines (BPL) networks; Power Line Communications (PLC); Faults; Fault Analysis; Transmission Power Grids

1. Introduction

The deployment of broadband over power lines (BPL) networks across the traditional overhead high-voltage (OV HV) power grid provides a plethora of advantages that render these networks both a useful power grid complement and a strong telecommunications competitor to wireless networking solutions [1]-[4]. Among the characteristics of the emerging power network, some of them that deserve special attention are: (i) its IP-based communications network capabilities; (ii) a great number of smart grid applications; (iii) the low-cost deployment; and (iv) the potential of broadband last mile access through its wired/wireless interfaces due to the power grid ubiquitousness [5]-[13].

*Corresponding author: AGLazaropoulos@gmail.com

Tr Ren Energy, 2016, Vol.2, No.3, 85-112. doi: 10.17737/tre.2016.2.3.0026

Nevertheless, when considered as a medium for the transmission of communications signals, OV HV BPL networks are subjected to various inherent deficiencies such as high and frequency-selective channel attenuation and noise [5], [8], [14]-[17]. The broadband potential of OV HV BPL networks is significantly influenced by each of the aforementioned insidious factors [18], [19].

As the channel attenuation is concerned in this paper, the well-established hybrid method, which is employed to examine the behavior of multiconductor transmission line (MTL) structures, is also adopted in this paper [5]-[7], [14]-[17], [20]-[27]. Successfully tested in various transmission and distribution BPL networks [8], [24], [28], the hybrid method is based on: (i) a bottom-up approach that consists of the MTL theory, eigenvalue decomposition (EVD) and singular value decomposition (SVD) [7], [14], [18], [22], [25], [27], [29], [30]; and (ii) a top-down approach that is denoted as TM2 method and is based on the concatenation of multidimensional chain scattering matrices [5]-[7], [14]-[17], [20]-[22], [26], [29]. When the OV HV BPL network topology, OV HV MTL configuration and the applied coupling scheme are given as inputs, the hybrid method gives as an output the corresponding transfer function. In this paper, an OV HV BPL transfer function database is created where all the possible OV HV BPL network topologies are recorded as well as their corresponding transfer functions.

Despite the fact that a plethora of experimental results and theoretical analyses validate the theoretical accuracy of the hybrid method [16], [17], [31], [32], a number of practical reasons and “real-life” conditions may create measurement differences between experimental and theoretical results during the transfer function determination of OV HVBPL network topologies. On the basis of six measurement difference categories, which are analytically reported in the following analysis, their impact on the transfer functions of transmission BPL networks is evaluated and analyzed. In accordance with [1], to mitigate the aforementioned measurement differences and restore the underlaid theoretical transfer function, best L1PMA has been successfully applied in distribution BPL networks. Among the myriad of data approximation methods that has been proposed in the literature, the application of the best L1PMA, which is theoretically presented and experimentally verified in [33]-[39], is adopted in this paper. Due to its remarkable efficiency to cope with the measurement differences of distribution BPL networks [1], best L1PMA is first applied during the revelation of theoretical OV HV BPL transfer functions. By recognizing the theoretical OV HV BPL transfer function, the respective OV HV BPL network topology can be identified through its curve similarity with the available records of the OV HV BPL transfer function database.

The rest of this paper is organized as follows: In Sec. II, the OV HV MTL configuration and the respective indicative topologies are presented. Sec. III summarizes the principles of BPL signal transmission through the lens of the well-validated hybrid method. The creation procedure of the OV HV BPL transfer function database is also detailed. In Sec.IV, a presentation of the best L1PMA is given. Implementation details, mathematical analysis and the appropriate curve similarity performance metric (CSPM) concerning best L1PMA are analytically reported. Sec.V discusses the simulations of various transmission BPL networks intending to mark out the efficiency of the proposed topology identification methodology (TIM) either to mitigate the occurred measurement differences or to identify OV HV BPL network topologies. Sec.VI concludes this paper.

2. Transmission Power Grids

2.1 OV HV MTL Configuration

A typical OV 400kV double-circuit MTL configuration is depicted in Fig. 1 [6], [8]. This OV HV MTL configuration consists of eight conductors ($n^{\mathrm{OVHV}}=8$) that are divided into two categories, namely:

- *Phase lines*: These lines with radii $r_{\mathrm{p}}^{\mathrm{OVHV}}$=15.3mm are hung at typical heights $h_{\mathrm{p}}^{\mathrm{OVHV}}$ equal to 20m above ground –i.e., conductors 1, 2, 3, 4, 5, and 6–. The six phase conductors of the OV HV MTL configuration are further divided into three bundles; the phase conductors of each bundle are connected by non-conducting spacers and are separated by $\Delta_{\mathrm{p2}}^{\mathrm{OVHV}}$ equal to 400mm, whereas bundles are spaced by $\Delta_{\mathrm{p1}}^{\mathrm{OVHV}}$ equal to 10m.
- *Neutral conductors*: Except for the phase conductors, two parallel neutral conductors, which are the conductors 7 and 8, are hung at heights $h_{\mathrm{n}}^{\mathrm{OVHV}}$ equal to 23.7m. The neutral conductors with radii $r_{\mathrm{n}}^{\mathrm{OVHV}}$=9mm are spaced by $\Delta_{\mathrm{n}}^{\mathrm{OVHV}}$ equal to 12m.

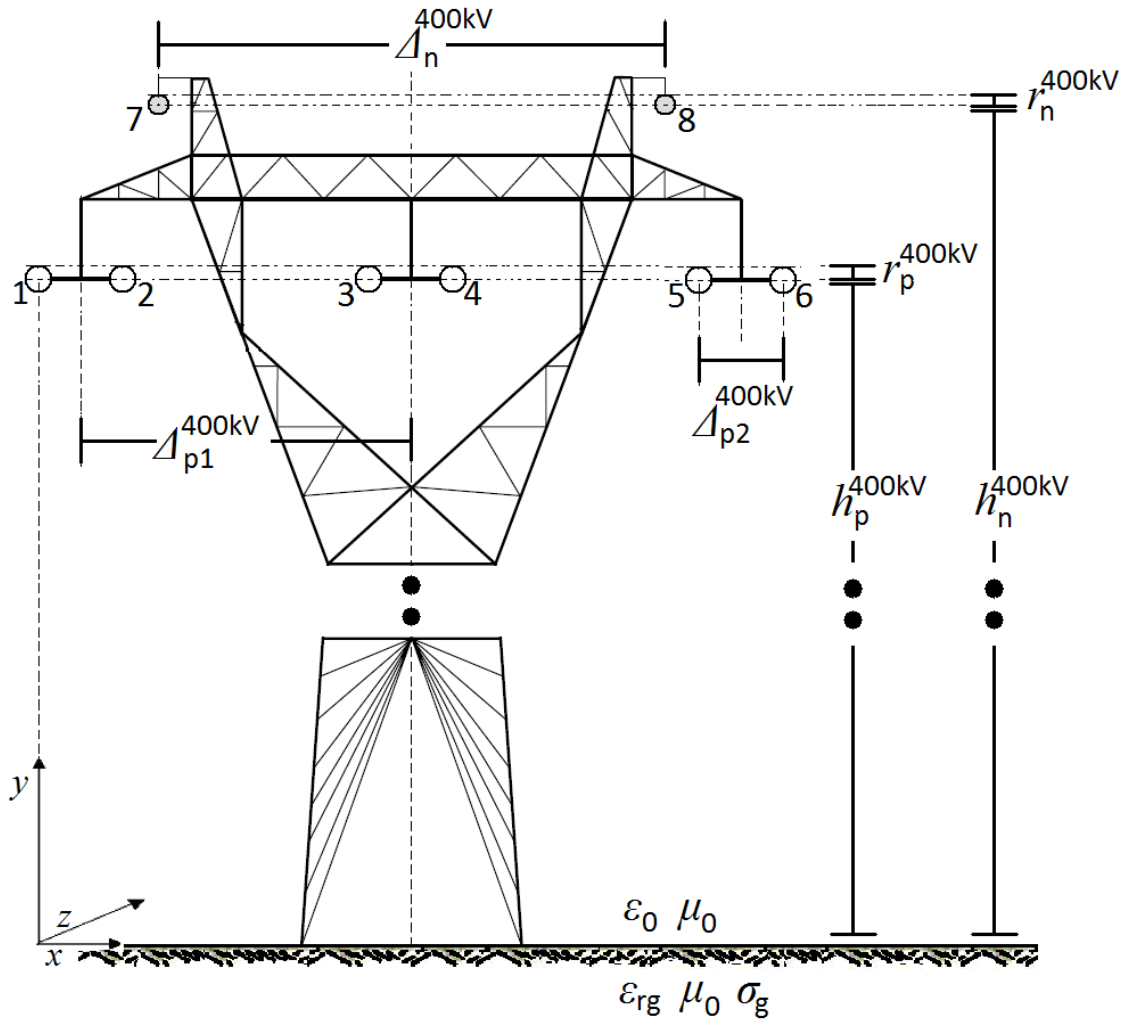

Figure 1.OV 400kV double-circuit MTL configuration [6], [8].

In accordance with [5], [6], [8], [40], [41], the ground with conductivity σ_g =5mS/m and relative permittivity ε_{rg} =13 is considered as the reference conductor. The aforementioned ground parameters define a realistic scenario during the following analysis while the impact of imperfect ground on broadband signal propagation via OV HV power lines was analyzed in [5], [6], [14]-[17], [21], [25], [40], [42], [43].

2.2 Indicative OV HV BPL Topologies

Since OV HV BPL networks suffer from various inherent deficiencies such as high and frequency-selective channel attenuation and noise, BPL networks are divided into cascaded BPL topologies in order to cope with these deficiencies [1], [5], [8], [14]-[17], [44], [45]. Each OV HV BPL topology, which is denoted as network module, is bounded by the transmitting and receiving end where respective BPL repeaters are installed. The role of BPL repeaters is to extract the attenuated BPL signal, amplify it while improving its signal-to-noise ratio and inject it in OV HV lines. Between the two BPL repeaters of each OV HV BPL topology, N successive branches are encountered.

According to the previous description, a general OV HV BPL topology is presented in Fig. 2.

In accordance with [5]-[7], [14]-[17], [20]-[26], [29], [40], [46], [47] and with reference to Fig. 2, average path lengths of the order of 25km are considered in OV HV BPL topologies. The following three indicative OV HV BPL topologies, concerning end-to-end connections of average path lengths, are examined, namely [5], [6]:

1. A typical suburban topology (OV HV suburban case) with N=2 branches (L_1=9km, L_2=13km, L_3=3km, L_{b1}=17km, L_{b2}=13km).
2. A typical rural topology (OV HV rural case) with only N=1 branch (L_1=4km, L_2=21km, L_{b1}=24km).
3. The "LOS" transmission along the same end-to-end distance $L=L_1+\ldots+L_{N+1}$=25km when no branches are encountered. This topology corresponds to Line of Sight transmission in wireless channels.

The three indicative OV HV BPL topologies are going to be used so that the accuracy of the proposed TIM is evaluated in Sec.V.

As the circuital parameters of OV HV BPL topologies are regarded [5]-[7], [14]-[17], [20]-[26], [29], [40], [41], [46], [47], several assumptions need to be taken into account: (i) The branching cables are assumed identical to the transmission cables; (ii) The interconnections between the transmission and branch conductors are fully activated; (iii) The transmitting and the receiving ends are assumed matched to the characteristic impedance of the modal channels; and (iv) The branch terminations are assumed open circuits.

2.3 OV HV BPL Topologies of the Proposed Database

As it has already been mentioned in Sec.IIB, average path lengths L of the order of 25km are considered in OV HV BPL topologies. To create a detailed OV HV BPL topology database, all the possible OV HV BPL topologies concerning the number of branches, branch distance from the transmitting end and branch length need to be inserted in the database. In order to simplify the following analysis without harming the generality of the proposed TIM, the maximum number of branches, the length spacing for both branch distance and branch length and the maximum branch length are assumed to be equal to N, L_s in km and L_b in km, respectively. Therefore, the following cases are reported for each number of branches with reference to Fig. 2:

- 1 topology when no branches are encountered (i.e., "LOS" transmission case).
- When one branch is assumed, there are L/L_s+1 possible branch locations for the length L_1 across the "LOS" transmission path. Here, it should be noted that the branch may also be located either at the transmitting (L_1=0km) or at the receiving end (L_1=L). If the L_b/L_s+1 possible branch lengths of the length L_{b1} are considered then $\left(\frac{L}{L_s}+1\right)\times\left(\frac{L_b}{L_s}+1\right)$ topologies of one branch should be inserted in the OV HV BPL topology database.
- When two branches are assumed, let the first branch be located at distance L_1 from the transmitting end. To avoid duplicates in the OV HV BPL topology database, the second branch can be located at distance L_2 from the first branch

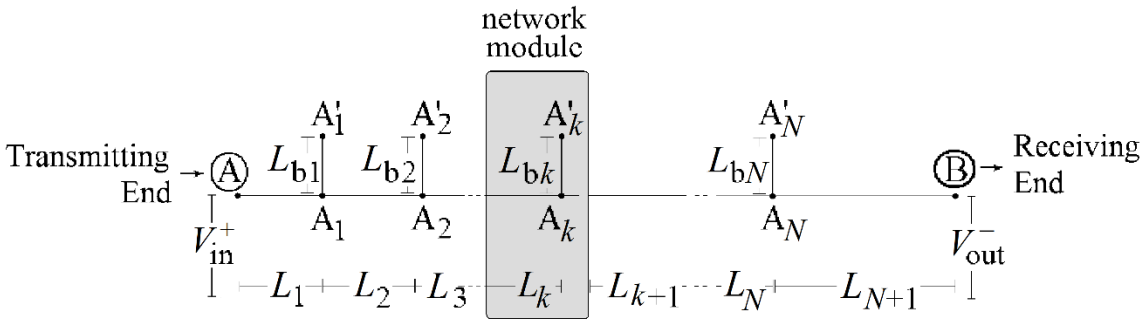

Figure 2. General OV HV BPL topology [6], [8].

that varies from 0 (double branch) to L-L_1. Since the average path length is assumed equal to L in all the cases examined, the length L_3 is equal to L-L_1-L_2. If the branch length L_{b1} and L_{b2} are also taken into account then the number of possible OV HV BPL topologies, which is inserted in the OV HV BPL topology database, is equal to $\sum_{i_1=1}^{L/L_s+1} i \times \left(\frac{L_b}{L_s}+1\right)^2$.

- Similarly to the two branch case, when N branches are considered across the "LOS" transmission path, there are

$$\sum_{i_1=1}^{L/L_s+1}\left\{\sum_{i_2=1}^{i_1}\left\{\cdots\sum_{i_{N-1}=1}^{i_{N-2}}\{i_{N-1}\}\right\}\right\}\times\left(\frac{L_b}{L_s}+1\right)^N \quad (1)$$

possible OV HV BPL topologies that should be inserted in the OV HV BPL topology database.

Since all the possible OV HV BPL topologies are inserted in the database as separate records, each record is accompanied by: (i) its theoretical OV HV BPL transfer function by applying the hybrid method, whose evaluation is detailed in Sec.IIIB and IIIC; and (ii) its approximated OV HV BPL transfer functions by applying the best L1PMA, whose evaluation is detailed in Sec.IVC.

3. A Briefing of BPL Propagation and Transmission Analysis

3.1 MTL Theory

As it has already been mentioned in [5]-[7], [14]-[17], [20]-[22], [25], [40], [44], through a matrix approach, the standard TL analysis can be extended to the MTL case. In the traditional case of a two-conductor line, one forward- and one backward-traveling wave are supported. However, in the MTL case where the MTL structure consists of n^{OVHV}+1 conductors parallel to the z axis (see Fig. 1), n^{OVHV} pairs of forward- and backward-traveling waves with corresponding propagation constants may be supported. Each pair of forward- and backward-traveling waves is referred to as a mode and their OV HV spectral behavior has already been investigated in [5]-[7], [14]-[17], [20]-[22], [25]-[27], [29], [30], [40]-[44], [47], [48].

3.2 EVD Modal Analysis and Channel Transfer Functions

With reference to Fig.1, the n^{OVHV} modes, which are supported by the examined MTL configuration, may propagate across OV HV BPL topologies. Through TM2 method, which is based on the scattering matrix theory and presented analytically in [7], [22], their spectral behavior is described by the $n^{\mathrm{OVHV}} \times n^{\mathrm{OVHV}}$ EVD modal transfer function matrix $\mathbf{H}^{\mathrm{m}}\{\cdot\}$ whose elements $H_{i,j}^{\mathrm{m}}\{\cdot\}$, $i,j=1,\ldots,n^{\mathrm{OVHV}}$ are the EVD modal transfer functions where $H_{i,j}^{\mathrm{m}}$ denotes the element of matrix $\mathbf{H}^{\mathrm{m}}\{\cdot\}$ in row i of column j. Through appropriate similarity transformations, which are presented in [5]-[7], [14]-[17], [20]-[22], [25], [40], [44], the EVD modal transfer functions are related with the line transfer functions through the $n^{\mathrm{OVHV}} \times n^{\mathrm{OVHV}}$ channel transfer function matrix $\mathbf{H}\{\cdot\}$ that is determined from

$$\mathbf{H}\{\cdot\} = \mathbf{T}_V \cdot \mathbf{H}^m\{\cdot\} \cdot \mathbf{T}_V^{-1} \tag{2}$$

where $\mathbf{T}_V$ is a $n^{\mathrm{OVHV}} \times n^{\mathrm{OVHV}}$ matrix depending on the frequency, the MTL configuration and the physical properties of the cables.

3.3 Coupling Schemes and Coupling Transfer Functions

According to how signals are injected into OV HV lines, two coupling schemes are mainly supported by the OV HV BPL networks, as folows [6], [7], [11], [12], [28]:

- *Wire-to-Ground* (WtG) when the signal is injected into one conductor and returns via the ground; say between conductor s,s=1,...,8 and the ground. The coupling WtG channel transfer function $H^{\mathrm{WtG}}\{\cdot\}$ is given from

$$H^{\mathrm{WtG}}\{\cdot\} = \left[\mathbf{C}^{\mathrm{WtG}}\right]^{\mathrm{T}} \cdot \mathbf{T}_V \cdot \mathbf{H}^m\{\cdot\} \cdot \mathbf{T}_V^{-1} \cdot \mathbf{C}^{\mathrm{WtG}} \tag{3}$$

  where $\mathbf{C}^{\mathrm{WtG}}$ is an 8×1 coupling column vector with zero elements except in row s where the value is equal to 1. WtG coupling between conductor s and ground will be detoned as WtG^s, hereafter.
- *Wire-to-Wire* (WtW) when the signal is injected between two conductors; say between conductors p and $q \neq p$, p,q=1,…,8. Similarly to eq. (3), the coupling WtW channel transfer function $H^{\mathrm{WtW}}\{\cdot\}$ is given from

$$H^{\mathrm{WtW}}\{\cdot\} = \left[\mathbf{C}^{\mathrm{WtW,out}}\right]^{\mathrm{T}} \cdot \mathbf{T}_V \cdot \mathbf{H}^m\{\cdot\} \cdot \mathbf{T}_V^{-1} \cdot \mathbf{C}^{\mathrm{WtW,in}} \tag{4}$$

  where $\mathbf{C}^{\mathrm{WtW,out}}$ and $\mathbf{C}^{\mathrm{WtW,in}}$ are 8×1 output and input coupling column vectors, respectively.

Since the main interest of this paper is the accuracy evaluation of the proposed TIM, only one of the previous coupling schemes is going to be applied in the following analysis for the sake of clarity and terseness; say, WtG coupling schemes.

4. Best L1PMA

4.1 Best L1PMA and BPL Networks

Among the various proposed monotonic data approximation methods, the application of the best L1PMA, which is theoretically presented and experimentally verified in [33]-[38], successfully copes with problems that are derived from the

univariate signal restoration such as those presented during the BPL transfer function determination. Until now, the efficacy of best L1PMA to mitigate measurement differences during the determination of distribution BPL transfer functions has already been verified in [1]. In this paper, best L1PMA is first applied to OV HV BPL transfer functions either to mitigate the occurred measurement differences or to identify OV HV BPL topologies.

4.2 Implementation Details

Contrary to spline and wavelet approximation methods [49], [50], best L1PMA avoids the assumption that BPL transfer functions depend on certain critical parameters. Actually, the smoothing process is a straightforward data projection when best L1PMA is adopted [1], [34], [35].

Best L1PMA exploits the piecewise monotonicity property that always occurs in transmission and distribution BPL transfer functions [1]. Best L1PMA decomposes BPL transfer functions into separate monotonous sections between adjacent turning points (primary extrema) of the examined transfer functions [35], [36]. By identifying the separate monotonous sections, best L1PMA separately handles them, thus, achieving very good results especially concerning the mitigation of uncorrelated measurement differences [1], [51]. Since best L1PMA is based on the minimization of the moduli sum of the measurement differences, the existence of few large measurement differences among the data make no difference to the best fit [51]. Therefore, the undulation of the OV HV BPL coupling transfer function data due to the existence of deep spectral notches and other measurement differences can be comfortably accommodated through the application of the best L1PMA.

Apart from its easy theoretical implementation concept, another basic advantage of the best L1PMA is its software availability and comprehensibility. The Fortran software package that is applied to implement the best L1PMA has extensively been verified in various scientific fields [36], [38], [52]-[54] and is freely available online in [39]. As the easiness plays critical role, based on the best L1PMA software specifications of [39], best L1PMA receives as inputs the measured OV HV BPL coupling transfer function, the measurement frequencies, the number of monotonic sections (i.e., either user- or computer-defined) and the type of the first monotonic section (i.e., either increasing or decreasing). Then, by executing the Fortran software package, which is a straightforward procedure, the outputs of best L1PMA are the optimal primary extrema and the best fit of the measured OV HV BPL coupling transfer function.

4.3 The Nature of Measurement Differences and Best L1PMA Mathematical Analysis

As already been mentioned, a set of practical reasons and “real-life” conditions create significant differences between experimental measurements and theoretical results during the transfer function determination of BPL networks. The reasons for these measurement differences can be grouped into six categories, namely [1], [55]-[57]: (i) Isolation difficulties of specific MTL parameters in time- and frequency-domain; (ii) Low accuracy and sensitivity of the used equipment during measurements; (iii) Cross-talk and resonant phenomena due to the parasitic capacitances and inductances of OV HV lines; (iv) The weakness of including specific wiring and grounding practices;

(v) Practical impedance deviations of OV HV lines, branches, terminations and transmitting/receiving ends; and (vi) The isolation lack of the noise effect during the transfer function computations. Taking under consideration the six measurement difference categories and eq. (4), the measured OV HV coupling transfer function $\overline{H^{\mathrm{WtG}}}\{\cdot\}$ is then determined by

$$\overline{H^{\mathrm{WtG}}}(f_i) = H^{\mathrm{WtG}}(f_i) + e(f_i) \tag{5}$$

where f_i denotes the measurement frequency and $e(f_i)$ synopsizes the total measurement difference due to the aforementioned six categories.

Generalizing eq. (5), the theoretical OV HV coupling transfer functions $H^{\mathrm{WtG}}(f_i)$, i=1,…,u with respect to measurement frequencies f_i, i =1,…,u are regarded as elements of $\mathbf{H}^{\mathrm{WtG}}$ where

$$\mathbf{H}^{\mathrm{WtG}} \equiv \mathbf{H}^{\mathrm{WtG}}(\mathbf{f}) = \left[H^{\mathrm{WtG}}(f_1) \quad \cdots \quad H^{\mathrm{WtG}}(f_i) \quad \cdots \quad H^{\mathrm{WtG}}(f_u)\right]^{\mathrm{T}} \tag{6}$$

is the $u\times1$ theoretical OV HV coupling transfer function column vector and $\mathbf{f} = \left[f_1 \quad \cdots \quad f_i \quad \cdots \quad f_u\right]^{\mathrm{T}}$ is the $u\times1$ measurement frequency column vector. Similarly, the measured OV HV coupling transfer functions $\overline{H^{\mathrm{WtG}}}(f_i)$, i=1,…,u with respect to measurement frequencies f_i, i =1,…,u are regarded as elements of $\overline{\mathbf{H}^{\mathrm{WtG}}}$ where

$$\overline{\mathbf{H}^{\mathrm{WtG}}} \equiv \overline{\mathbf{H}^{\mathrm{WtG}}}(\mathbf{f}) = \left[\overline{H^{\mathrm{WtG}}}(f_1) \quad \cdots \quad \overline{H^{\mathrm{WtG}}}(f_i) \quad \cdots \quad \overline{H^{\mathrm{WtG}}}(f_u)\right]^{\mathrm{T}} \tag{7}$$

is the $u\times1$ measured OV HV coupling transfer function column vector. Thus, with reference to Sec.IIIC, best L1PMA receives as inputs the measured OV HV coupling transfer function column vector $\overline{\mathbf{H}^{\mathrm{WtG}}}(\mathbf{f})$, the measurement frequencies $\mathbf{f}$, the number of monotonic sections k_{sect} and the type of the first monotonic section while best L1PMA gives as outputs the optimal primary extrema and the approximated OV HV coupling transfer function column vector $\overline{\overline{\mathbf{H}^{\mathrm{WtG}}_{\mathrm{meas}}}}(\mathbf{f}, k_{\mathrm{sect}})$ by minimizing the sum of the absolute errors

$$Er\left(\overline{\mathbf{H}^{\mathrm{WtG}}}, k_{\mathrm{sect}}\right) = \sum_{i=1}^{u} \left| \overline{\overline{\mathbf{H}^{\mathrm{WtG}}_{\mathrm{meas}}}}(f_i, k_{\mathrm{sect}}) - \overline{\mathbf{H}^{\mathrm{WtG}}}(f_i) \right| \tag{8}$$

subject to the piecewise monotonicity constraints

$$\left.\begin{aligned} &\overline{\overline{\mathbf{H}^{\mathrm{WtG}}_{\mathrm{meas}}}}\left(f_{\phi_{j-1}}, k_{\mathrm{sect}}\right) \le \overline{\overline{\mathbf{H}^{\mathrm{WtG}}_{\mathrm{meas}}}}\left(f_{\phi_{j-1}+1}, k_{\mathrm{sect}}\right) \le \cdots \le \overline{\overline{\mathbf{H}^{\mathrm{WtG}}_{\mathrm{meas}}}}\left(f_{\phi_j}, k_{\mathrm{sect}}\right), \text{if } j \text{ is odd} \\ &\overline{\overline{\mathbf{H}^{\mathrm{WtG}}_{\mathrm{meas}}}}\left(f_{\phi_{j-1}}, k_{\mathrm{sect}}\right) \ge \overline{\overline{\mathbf{H}^{\mathrm{WtG}}_{\mathrm{meas}}}}\left(f_{\phi_{j-1}+1}, k_{\mathrm{sect}}\right) \ge \cdots \ge \overline{\overline{\mathbf{H}^{\mathrm{WtG}}_{\mathrm{meas}}}}\left(f_{\phi_j}, k_{\mathrm{sect}}\right), \text{if } j \text{ is even} \end{aligned}\right\} \tag{9}$$

where the integer numbers ϕ_j, j= 1,…,k_{sect} define the positions of the primary extrema of the best L1PMA satisfying the conditions

$$1 = \phi_0 \le \phi_1 \le \cdots \le \phi_{k_{\mathrm{sect}}} = u \tag{10}$$

4.4 Best L1PMA and Theoretical OV HV Coupling Transfer Functions

Apart from its theoretical OV HV BPL coupling transfer function, each OV HV BPL topology is accompanied with a number of approximated theoretical OV HV BPL coupling transfer functions that come from the application of the best L1PMA for different monotonic sections. With reference to eqs. (8)-(10), the approximated

theoretical OV HV BPL coupling transfer function column vector $\overline{\overline{\mathbf{H}_{\text{theor}}^{\text{WtG}}}}(\mathbf{f},k_{\text{sect}})$ is the output of the best L1PMA when the measured OV HV BPL coupling transfer function column vector $\overline{\mathbf{H}^{\text{WtG}}}(\mathbf{f})$ is replaced by the theoretical one $\mathbf{H}^{\text{WtG}}(\mathbf{f})$ for given number of monotonic sections.

4.5 Traditional TIM

The traditional TIM is rather a rule of thumb than an accurate description. The traditional TIM is based on the minimization of the sum of the absolute errors between measured OV HV coupling transfer function column vector $\overline{\mathbf{H}^{\text{WtG}}}(\mathbf{f})$ and theoretical OV HV coupling transfer function column vector $\mathbf{H}^{\text{WtG}}(\mathbf{f})$, say

$$Er\left(\overline{\mathbf{H}^{\text{WtG}}},\mathbf{H}^{\text{WtG}}(\mathbf{f})\right)=\sum_{i=1}^{u}\left|\overline{\mathbf{H}^{\text{WtG}}}(f_i)-\mathbf{H}^{\text{WtG}}(f_i)\right| \tag{11}$$

and the belief that the underlaid OV HV BPL topology is the one that presents the minimum sum of eq. (11). However, this belief is far away the truth since the decision becomes more wrong as the maximum magnitude of measurement differences increases. Even if small measurement difference magnitudes are assumed, the OV HV BPL topology of the database that presents the minimum sum of eq. (11) rarely is the desirable one (see Sec.VE). In contrast, a successful TIM is the one that could give either the exact OV HV BPL topology, which is difficult due to the high number of OV HV BPL topologies of the database and different difference measurement magnitudes, or a set of candidate OV HV BPL topologies. Indeed, the proposed identification method offers a set of candidate OV HV BPL topologies where the desired OV HV BPL topology lays among them.

4.6 CSPM and the Proposed TIM

With reference to eqs. (8)-(10), best L1PMA gives the approximated OV HV coupling transfer function column vector $\overline{\overline{\mathbf{H}_{\text{meas}}^{\text{WtG}}}}(\mathbf{f},k_{\text{sect}})$ when measured OV HV one $\overline{\mathbf{H}^{\text{WtG}}}(\mathbf{f})$ and a number of monotonic sections k_{sect} are considered. The performance metric of the sum of the absolute errors, which is presented in eq. (8) and is, hereafter, denoted as CSPM, is also applied for the assessment of the curve similarity between the best L1PMA measurement approximation and theory, namely:

$$CSPM_{k_{\text{sec}\,t}}\equiv CSPM_{k_{\text{sec}\,t}}\left(\overline{\mathbf{H}^{\text{WtG}}},k_{\text{sect}}\right)=\sum_{i=1}^{u}\left|\overline{\overline{\mathbf{H}_{\text{meas}}^{\text{WtG}}}}(f_i,k_{\text{sect}})-\overline{\overline{\mathbf{H}_{\text{theor}}^{\text{WtG}}}}(f_i,k_{\text{sect}})\right| \tag{12}$$

The proposed TIM is based on the CSPM and the OV HV topology database in order to identify the OV HV BPL topology when a set of coupling transfer function measurements is available. Actually, the methodology follows the following three steps so that the OV HV BPL topology is revealed:

1. Given the measured OV HV coupling transfer function column vector $\overline{\mathbf{H}^{\text{WtG}}}(\mathbf{f})$, the approximated OV HV coupling transfer function column vector $\overline{\overline{\mathbf{H}_{\text{meas}}^{\text{WtG}}}}(\mathbf{f},k_{\text{sect}})$

is evaluated for monotonic sections that range from 1 to $k_{\text{sect,max}}$ where $k_{\text{sect,max}}$ is the maximum number of monotonic sections considered.

2. For each OV HV BPL topology and each monotonic section of the OV HV BPL topology database, the respective $CSPM_{k\text{sect}}$ of eq. (12) is computed. Then, for each OV HV BPL topology, the total $CSPM_{\text{tot}}$ is determined from

$$CSPM_{\text{tot}} \equiv \sum_{k_{\text{sect}}=1}^{k_{\text{sect,max}}} CSPM_{k_{\text{sec}\,t}} \tag{13}$$

3. A set of candidate OV HV BPL topologies with their respective $CSPM_{\text{tot}}$ is provided by the TIM. This set of candidates OV HV BPL topologies is characterized by the lowest $CSPM_{\text{tot}}$ among all the available OV HV BPL topologies of the database. The number of candidate OV HV BPL topologies depends on the topological characteristics of the underlaid topology (i.e., number of branches, branch length), the nature of measurement differences (i.e., measurement difference distributions, characteristics of distributions) and the number of monotonic sections applied.

As it is evident from the previous steps, CSPM acts either as a curve similarity metric or as a topology identification tool. Finally, the simulation results of the proposed TIM are shown in Sec.VE.

5. Numerical Results and Discussion

5.1 Simulation Goals and Parameters

Various types of transmission BPL networks are simulated with the purpose of evaluating the proposed TIM. More specifically, the efficiency of the methodology is assessed with reference to a number of factors, such as the transmission BPL topology and the nature of measurement differences.

As regards the hybrid method specifications, the BPL frequency range and the flat-fading subchannel frequency spacing are assumed equal to 1-30MHz and 1MHz, respectively. Therefore, the number of subchannels u in the examined frequency range is equal to 30. Arbitrarily, the WtG[3] coupling scheme is applied during the following simulations. As it is usually done [5], [20]-[23], [58], the selection of representative coupling schemes is a typical procedure for the sake of reducing manuscript size and simplicity.

As the OV HV BPL topology database specifications are concerned, the maximum number of branches N, the length spacing L_{s} for both branch distance and branch length and the maximum branch length L_{b} are assumed equal to 3, 1km and 25km, respectively.

Finally, the maximum number of monotonic sections $k_{\text{sect,max}}$ that is going to be used during the application of best L1PMA is assumed to be equal to 20 [1].

5.2 Theoretical and Approximated OV HV BPL Transfer Functions

Prior to understanding the proposed TIM, there is a need for recognizing: (i) how best L1PMA approximates theoretical coupling transfer functions of transmission OV BPL topologies, such those presented in Sec.IIB, and (ii) the role of the number of the monotonic sections during the OV HV BPL coupling transfer function approximation.

In Figs. 3(a)-(c), the theoretical coupling transfer function is plotted versus frequency for the three indicative OV HV BPL topologies of the Sec.IIB, respectively. In each figure, the best L1PMA result is also plotted for a number of representative monotonic sections (i.e., k_{sect}=2, k_{sect}=5 and k_{sect}=20). In Table 1, the average error between theoretical coupling transfer function and the respective best L1PMA output is reported for different number of monotonic sections when the three indicative OV HV BPL topologies are considered.

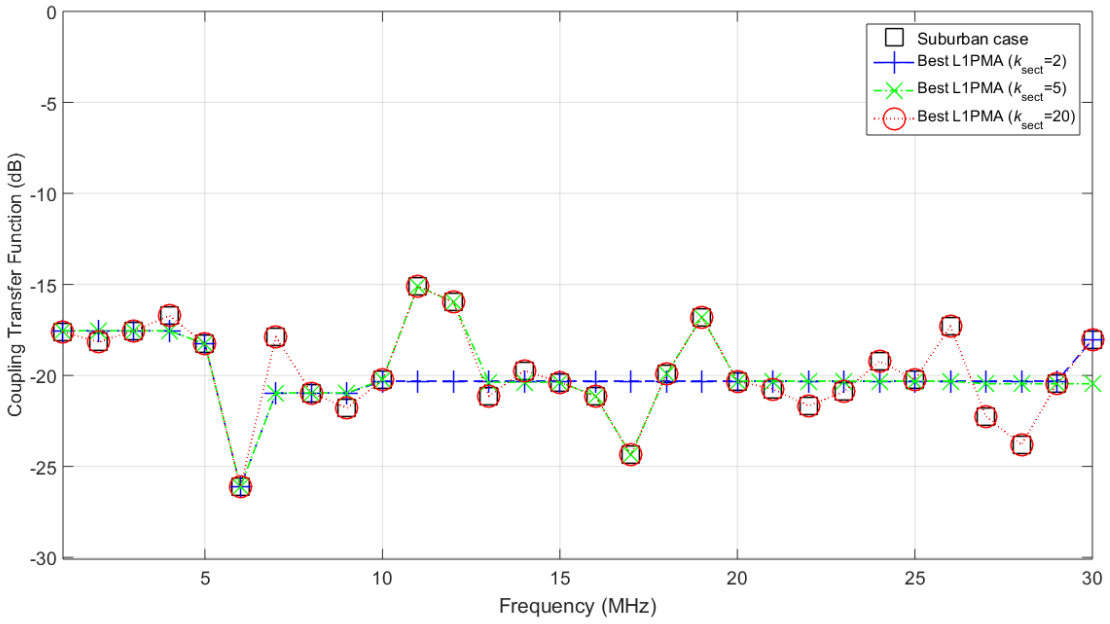
Suburban case
Best L1PMA (k_{sect}=2)
Best L1PMA (k_{sect}=5)
Best L1PMA (k_{sect}=20)
Coupling Transfer Function (dB)
Frequency (MHz)
0
-5
-10
-15
-20
-25
-30
5
10
15
20
25
30

(a)

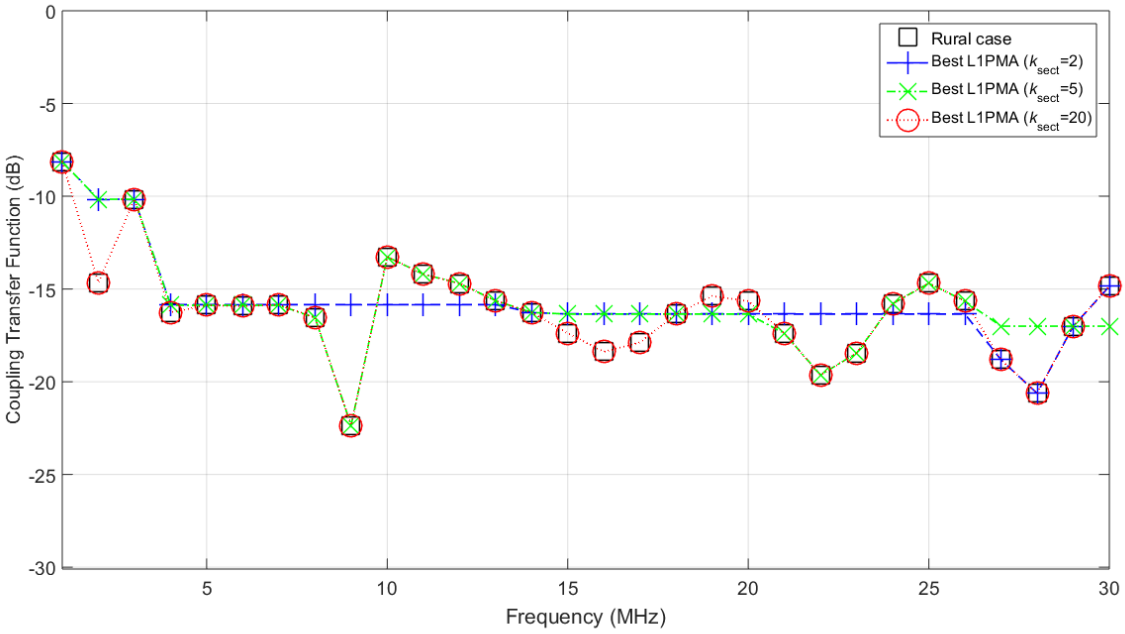
Rural case
Best L1PMA (k_{sect}=2)
Best L1PMA (k_{sect}=5)
Best L1PMA (k_{sect}=20)
Coupling Transfer Function (dB)
Frequency (MHz)
0
-5
-10
-15
-20
-25
-30
5
10
15
20
25
30

(b)

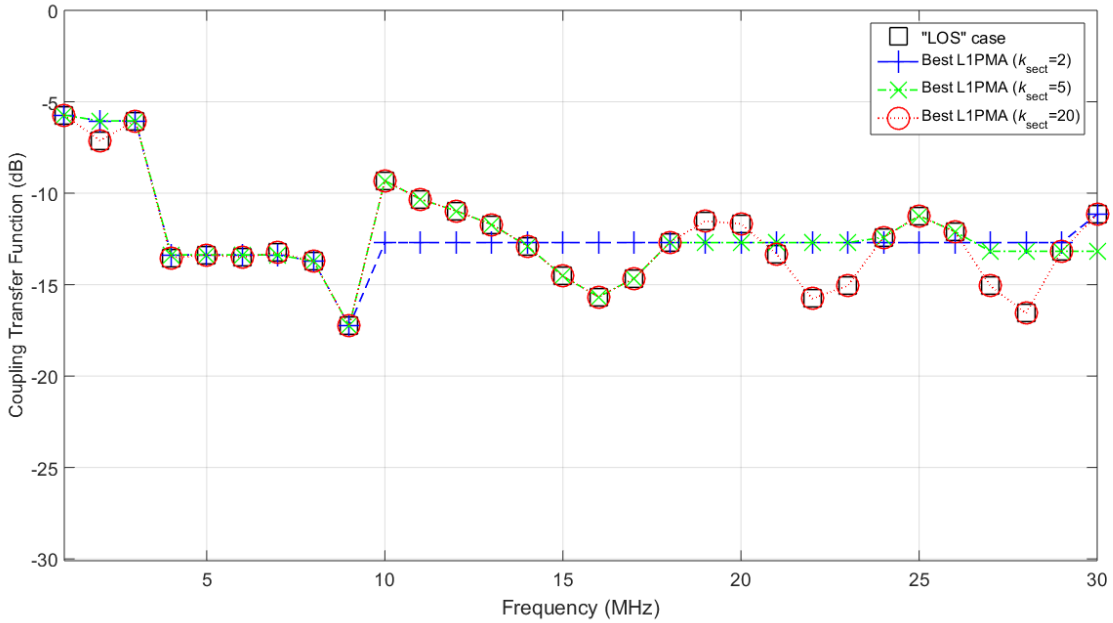

(c)

Figure 3. Theoretical and approximated coupling transfer functions of the three indicative topologies of OV HV BPL networks when best L1PMA is applied (a) Suburban case. (b) Rural case. (c) "LOS" case.

TABLE I
Average Errors between Theoretical and Approximated Coupling Transfer Functions

Number of Monotonic Sections	Average Error (dB)		
	Suburban case	Rural case	"LOS" case
1	0.08	0.29	-0.01
2	-0.23	0.44	0.26
3	-0.01	0.23	0.35
4	-0.10	0.38	0.31
5	-0.05	0.37	0.28
6	-0.14	0.26	0.17
7	-0.14	0.26	0.15
8	-0.04	0.16	0.04
9	-0.04	0.16	0.04
10	0.03	0.01	5.33×10^{-3}
11	0.03	0.01	5.33×10^{-3}
12	0.04	1.79×10^{-3}	4.26×10^{-3}
13	0.04	1.79×10^{-3}	4.26×10^{-3}
14	0.03	-2.26×10^{-7}	1.81×10^{-7}
15	0.03	-2.26×10^{-7}	1.81×10^{-7}
16	4.76×10^{-7}	-2.26×10^{-7}	1.81×10^{-7}
17	4.79×10^{-7}	-2.26×10^{-7}	1.81×10^{-7}
18	4.79×10^{-7}	-2.26×10^{-7}	1.81×10^{-7}
19	4.79×10^{-7}	-2.26×10^{-7}	1.81×10^{-7}
20	4.79×10^{-7}	-2.26×10^{-7}	1.81×10^{-7}

Comparing Figs. 3(a)-(c) with Table 1, several interesting remarks can be pointed out, as follows:

- As already been observed in distribution BPL networks [1], best L1PMA may successfully approximate the coupling transfer functions in all the OV HV BPL topologies examined, namely:
    - "LOS" case is characterized by coupling transfer functions with few and shallow spectral notches. Due to the proximity of the conductors with reference to their height above the ground, significant cross-talk phenomena arise between the conductor couples of the same phase having as a result the presence of notches even during the "LOS" transmission case. Anyway, best L1PMA curves practically coincide with the "LOS" coupling transfer functions. In fact, only eight monotonic sections are required so that the coincidence clearly occurs. Note that the threshold of the coincidence is assumed equal to 0.1dB.
    - Rural topologies are characterized by shallow and less-frequent spectral notches. Actually, because of their high branch length, OV HV BPL rural topologies act as power dividers of the "LOS" one, adding an approximately 3dB decrease in their coupling transfer functions for each branch encountered [7]. Therefore, the poor multipath environment of both "LOS" and rural topologies allows to the best L1PMA to achieve an excellent approximation in both cases with low number of monotonic sections. Indeed, best L1PMA achieves to follow the curve from the first monotonic section while the coincidence occurs after ten monotonic sections.
    - Suburban and urban topologies are characterized by deep and frequent spectral notches that pose a significant approximation challenge to the best L1PMA [1], [6]. This is due to the fact the branch length becomes short enough so that the channel attenuation of the different multipath paths during the BPL signal transmission become comparable, thus, creating a rich multipath environment. In fact, the spectral notches are added to the OV HV BPL coupling transfer functions of the "LOS" topology. Even in the bad case of the suburban topology, best L1PMA achieves to coincide with the OV HV coupling transfer functions after 16 monotonic sections.
- In contrast with wavelet or spline approximations [1], [49], [50], best L1PMA result successfully includes either the primary extrema or the tail of the OV HV coupling transfer functions.

With reference to Table 1, even from the first monotonic section, the best L1PMA achieves an average error that is equal to 0.08dB, 0.29dB and -0.01dB for the suburban, rural and "LOS" case, respectively. This indicates that best L1PMA identifies and follows the crucial areas of OV HV BPL coupling functions whose neglect significantly affects the average error. At the same time, best L1PMA disregards the frequent fluctuations whose contribution to the average error remains topically and low. In reality, this is the cornerstone of the TIM; the measurement differences are ignored by the best L1PMA while the curve essence of the OV HV BPL coupling transfer functions remains.

5.3 OV HV BPL Topology Database and Computational Load

With reference to Sec. IIC, to create a detailed OV HV BPL topology database, all the possible OV HV BPL topologies concerning the number of branches, each branch distance from the transmitting end and each branch length need to be added in the database. Taking under consideration the OV HV BPL topology database specifications of Sec.VA, there is a need for inserting 20 approximated theoretical OV HV BPL coupling transfer function column vectors per each possible OV HV BPL topology of the database, which corresponds to the respective 20 monotonic sections. Note that each approximated theoretical OV HV BPL coupling transfer function column vector consists of 30 elements, which corresponds to the respective 30 measurement frequencies. Therefore, the detailed OV HV BPL topology database comprises:

- *"LOS" transmission case*: 1 topology and 1×20=20 corresponding approximated theoretical OV HV BPL coupling transfer function column vectors. In total, 600 elements are required to be inserted in the database.
- *OV HV BPL topologies with one branch*: With reference to eq. (1), there are 676 topologies and 13,520 corresponding approximated theoretical OV HV BPL coupling transfer function column vectors. In total, 405,600 elements are required to be inserted in the database.
- *OV HV BPL topologies with two branches*: With reference to eq. (1), there are 237,276 topologies and 4,745,520 corresponding approximated theoretical OV HV BPL coupling transfer function column vectors. In total, 142,365,600 elements are required to be inserted in the database.
- *OV HV BPL topologies with N branches*: With reference to eq. (1), there are $\sum_{i_1=1}^{26}\left\{\sum_{i_2=1}^{i_1}\left\{\cdots\sum_{i_{N-1}=1}^{i_{N-2}}\{i_{N-1}\}\right\}\right\}\times 26^N$ and $\sum_{i_1=1}^{26}\left\{\sum_{i_2=1}^{i_1}\left\{\cdots\sum_{i_{N-1}=1}^{i_{N-2}}\{i_{N-1}\}\right\}\right\}\times 26^N\times 20$ corresponding approximated theoretical OV HV BPL coupling transfer function column vectors. In total, $\sum_{i_1=1}^{26}\left\{\sum_{i_2=1}^{i_1}\left\{\cdots\sum_{i_{N-1}=1}^{i_{N-2}}\{i_{N-1}\}\right\}\right\}\times 26^N\times 600$ elements are required to be inserted in the database.

Practically, to create the OV HV BPL topology database, the computational load of only inserting the elements of the "LOS" transmission case and OV HV BPL topologies with one branch is equal to 406,200 records or 7,886s. This implies that each record approximately requires 0.0194s so that both the hybrid method and the best L1PMA are applied and the element insertion is complete. In Table 2, the number of elements and the approximated time duration of inserting OV HV BPL topologies of different number of branches is reported. Note that as the technical characteristics of the system performing the simulations are concerned, it has an Intel Pentium 1.9GHz CPU and 4GB RAM.

From Table 2, it is evident that the approximated time duration poses significant technical difficulties during the consideration of OV HV BPL topologies with high number of branches in the database. In fact, when the number of branches is equal or greater than four, the approximated time duration exceeds the year. These cases rarely occur in OV HV BPL topologies of average path length of 25km and for that reason are

TABLE II
Number of Elements and Approximated Time Duration of OV HV BPL Topologies

Number of Branches	Number of Elements	Approximated Time Duration (hours)
0	600	0.003
1	405,600	2.19
2	142,365,600	767.19
3	3.45×10^{10}	1.86×10^{5}
4	6.51×10^{12}	3.51×10^{7}
5	1.2×10^{15}	5.47×10^{9}

omitted in this paper. Anyway, as detailed in the Sec.IVH of [59], the optimization of the insertion methodology in OV HV BPL topology database is among the critical steps of the future research. In this paper, only the cases of "LOS" case and topologies with one branch are considered during the proposed TIM for the sake of simplicity and speed (see Sec.VE).

5.4 OV HV BPL Coupling Transfer Functions and Measurement Differences

As already been reported in Sec.IVB, there are six categories that can create significant measurement differences between measurements and theoretical results during the determination of OV HV BPL coupling transfer functions. Based on the hybrid method and best L1PMA, the theoretical OV HV BPL coupling transfer functions can be revealed even though significant measurement differences may occur. In fact, best L1PMA achieves to mitigate the additive measurement by simply maintaining the monotonicity pattern of each coupling transfer function, which is imposed by the number of monotonic sections. In accordance with [1], the total occurred fault due to the six measurement difference categories $e(\cdot)$, which is described in eq. (5), can be assumed to follow either continuous uniform distribution (CUD) with minimum value $-a_{\mathrm{CUD}}$ and maximum value a_{CUD} or normal distribution (ND) with mean m_{ND} and standard deviation s_{ND}.

The impact of measurement differences on the OV HV BPL coupling transfer functions is investigated in the subsection. More specifically, in Figs. 4(a)-(c), the theoretical coupling transfer function is plotted versus frequency for the indicative OV HV BPL topologies, respectively. In each figure, the measured coupling transfer function is also given when measurement differences follow the indicative measurement difference distributions: (i) CUD with a_{CUD}=3dB; and (ii) ND with m_{ND}=0dB and s_{ND}=2dB. Moreover, the result of best L1PMA is also curved for the measured coupling transfer function when six monotonic sections are assumed.

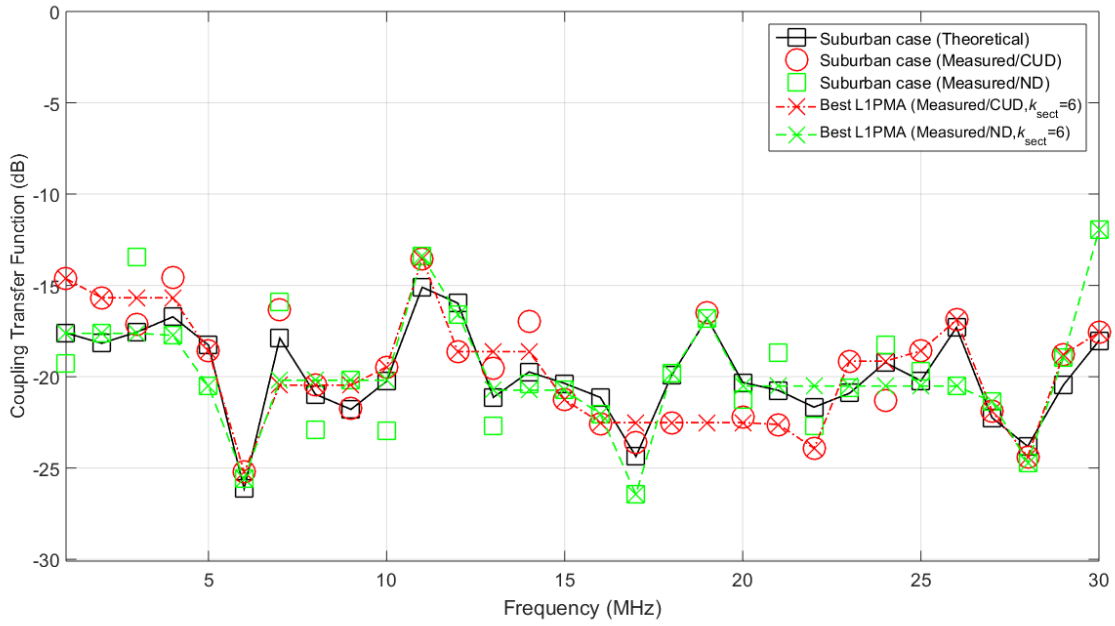
Suburban case (Theoretical)
Suburban case (Measured/CUD)
Suburban case (Measured/ND)
Best L1PMA (Measured/CUD,k_{sect}=6)
Best L1PMA (Measured/ND,k_{sect}=6)
Coupling Transfer Function (dB)
Frequency (MHz)
0
-5
-10
-15
-20
-25
-30
5
10
15
20
25
30

(a)

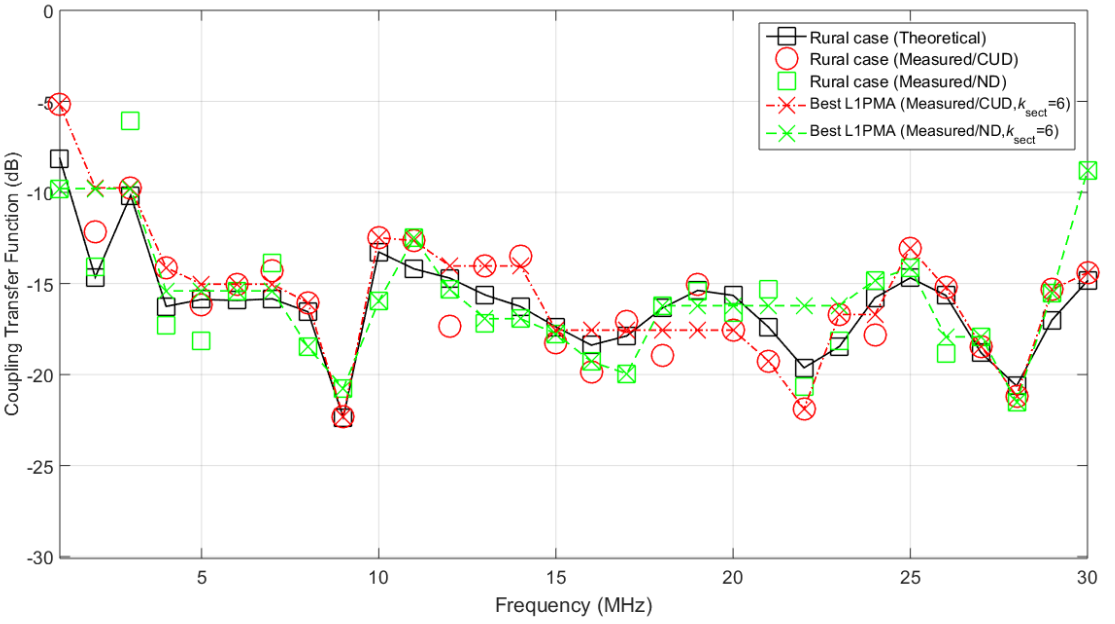
Rural case (Theoretical)
Rural case (Measured/CUD)
Rural case (Measured/ND)
Best L1PMA (Measured/CUD,k_{sect}=6)
Best L1PMA (Measured/ND,k_{sect}=6)
Coupling Transfer Function (dB)
Frequency (MHz)
0
-5
-10
-15
-20
-25
-30
5
10
15
20
25
30

(b)

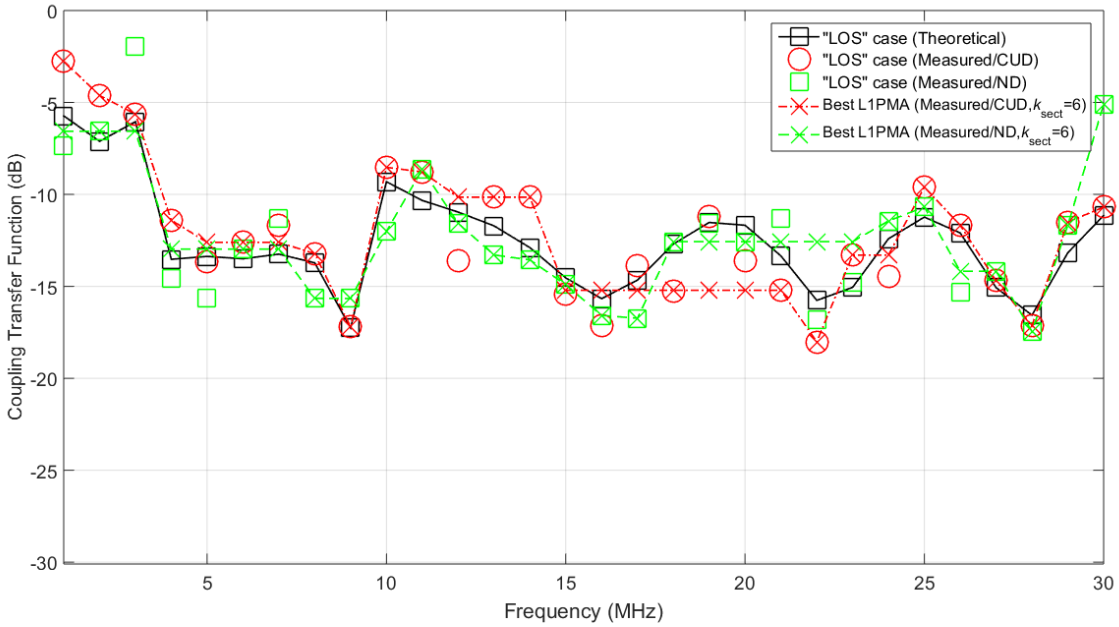

Figure 4. Theoretical, measured and approximated coupling transfer functions of the three indicative OV HV BPL topologies when best L1PMA is applied and two indicative fault distributions (CUD and ND) are adopted. (a) Suburban case. (b) Rural case. (c) "LOS" case.

From Figs. 3(a)-(c), it has been pointed out that best L1PMA first identifies the most important local extrema of the theoretical coupling transfer functions, which are treated as primary extrema. Then, best L1PMA interpolates the data at these extrema. The increase of the number of monotonic sections implies that the best L1PMA achieves to include even more secondary extrema in its results, thus, enhancing the accuracy of the approximation. From Figs. 4(a)-(c), it is obvious that the measurement differences, which may follow either CUD or ND, little affect the general form of the coupling transfer functions. Indeed, given the number of the monotonic sections, best L1PMA first tries to include the primary extrema of measured coupling transfer functions, which little differ from the respective primary extrema of the theoretical transfer functions, and second performs the best fit among the data in every monotonous section. In general terms, best L1PMA tries to restore the theoretical coupling transfer functions through its data smoothing capability.

5.5 TIM and the Set of Candidate OV HV BPL Topologies

As the restoration effectiveness of best L1PMA to theoretical and measured coupling transfer functions is well presented in the case of the indicative suburban, rural and "LOS" topologies, there are two significant drawbacks concerning the topology identification from the measured coupling transfer functions: (i) When a low number of monotonic sections is assumed, best L1PMA result follows the general trend of the respective measured coupling transfer function that resembles to the respective theoretical one but it loses significant primary extrema. (ii) When a high number of monotonic sections is assumed, best L1PMA result tends to identify both primary and

secondary extrema but exaggerates to include them, thus, giving important role to the measurement differences during the approximations. Taking into account the previous two performance tips, during the proposed TIM: (a) The TIM test is going to be applied between the approximated theoretical and measured coupling transfer functions for the same number of monotonic sections in both cases. (b) To exploit the advantages of the different number of monotonic sections, the TIM test includes the entire range of the available monotonic sections.

With reference to Sec.IVF, the three steps of the proposed TIM are now detailed:

1. The computation of measured OV HV coupling transfer function column vector $\overline{\mathbf{H}^{\mathrm{WtG}}}(\mathbf{f})$ and the approximated OV HV coupling transfer function column vector $\overline{\overline{\mathbf{H}_{\mathrm{meas}}^{\mathrm{WtG}}}}(\mathbf{f}, k_{\mathrm{sect}})$ for different number of monotonic sections has been presented in Sec.VD.
2. With reference to eq. (13), the OV HV BPL topology database of Sec.VC and the approximated measured OV HV BPL coupling transfer functions of Sec.VD, the $CSPM_{\mathrm{tot}}$ of the indicative topologies is calculated with respect to the topologies of the database. In Fig. 5(a), the $CSPM_{\mathrm{tot}}$ of the indicative rural topology and its position among the 677 OV HV BPL topologies of the database in ascending $CSPM_{\mathrm{tot}}$ order are plotted versus the CUD maximum value a_{CUD}. Apart from the proposed TIM, the respective position of the traditional TIM is also demonstrated. Similar curves with Fig. 5(a) are given in Fig. 5(b) but for different values of ND standard deviation s_{ND} when m_{ND} is equal to 0dB. In Figs. 5(c) and 5(d), similar curves with Figs. 5(a) and 5(b) are presented but for the indicative "LOS" topology.
3. A set of candidate OV HV BPL topologies with their respective $CSPM_{\mathrm{tot}}$ is provided by the TIM as it is shown in Figs. 5(a)-(d). All these topologies present the same $CSPM_{\mathrm{tot}}$ and coincide at the first position in ascending $CSPM_{\mathrm{tot}}$ order.

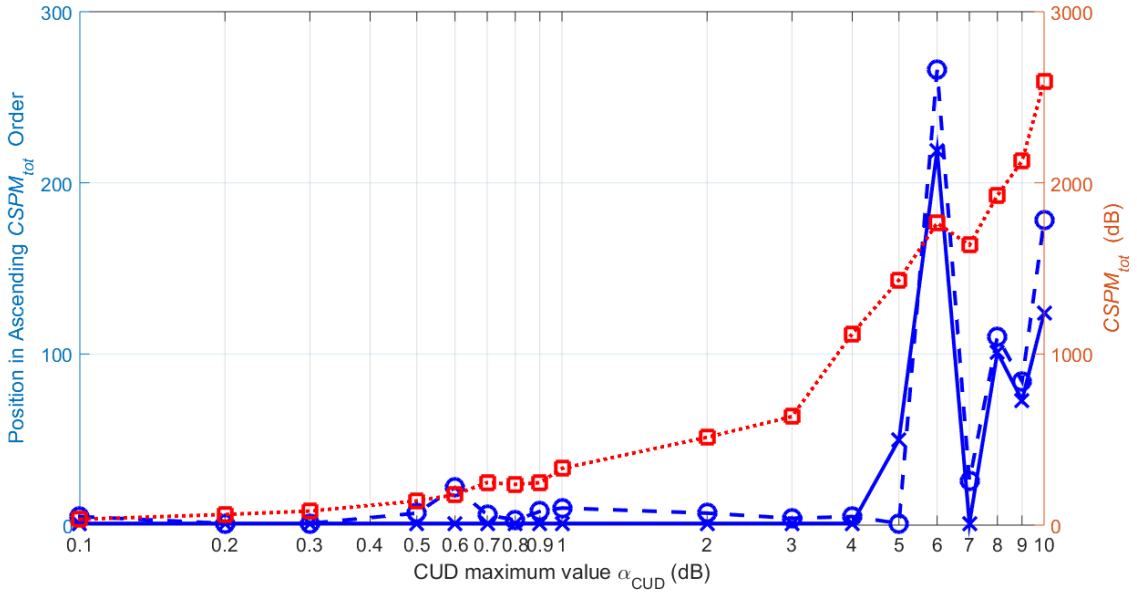
Position in Ascending $CSPM_{tot}$ Order
$CSPM_{tot}$ (dB)
CUD maximum value α_{CUD} (dB)
0.1 0.2 0.3 0.4 0.5 0.6 0.7 0.8 0.9 1 2 3 4 5 6 7 8 9 10
0 100 200 300
0 1000 2000 3000

(a)

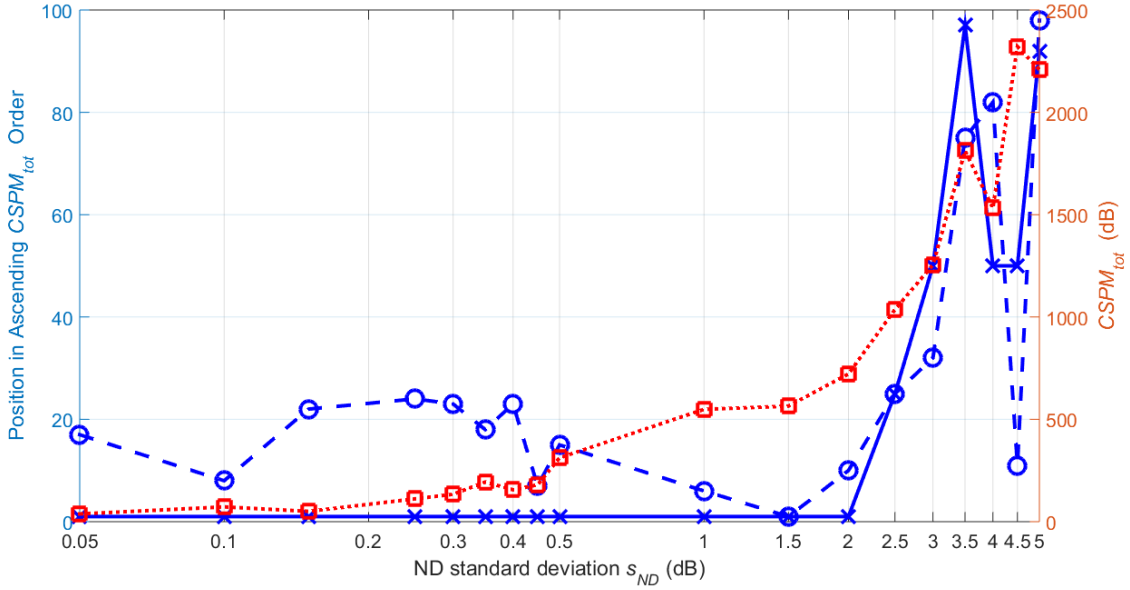
Position in Ascending $CSPM_{tot}$ Order
$CSPM_{tot}$ (dB)
ND standard deviation s_{ND} (dB)
0.05 0.1 0.2 0.3 0.4 0.5 1 1.5 2 2.5 3 3.5 4 4.5 5
0 20 40 60 80 100
0 500 1000 1500 2000 2500

(b)

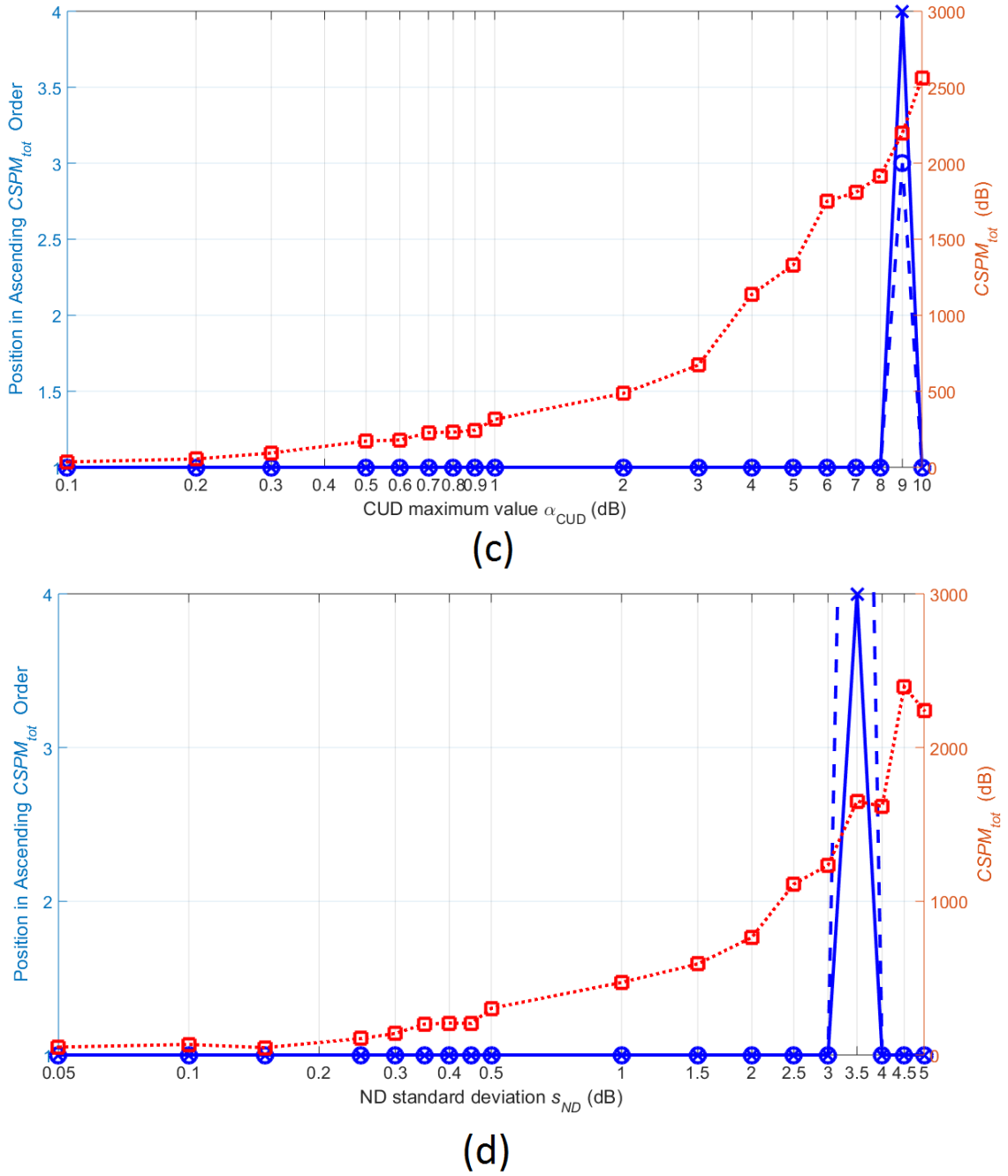

Figure 5. $CSPM_{tot}$ ( ) and position in ascending $CSPM_{tot}$ order versus measurement difference distribution characteristics when traditional TIM ( ) and proposed TIM ( ) are applied. (a) CUD / Rural case. (b) ND / Rural case. (c) CUD / "LOS" case. (d) ND / "LOS" case.

Observing Figs. 5(a)-(d), several interesting remarks concerning the TIM can be pointed out:

- "LOS" topology presents slightly lower CSPM values in comparison with the indicative rural ones. This is an obvious result since the additive spectral notches of the indicative rural topology challenge the efficiency of the proposed TIM in

contrast with the "LOS" case where its revelation from TIM is a straightforward procedure.

- The proposed TIM succeeds in identifying the underlaid OV HV BPL topology more precisely than traditional one in the vast majority of the cases examined. Actually, TIM successfully reveals the "LOS" and indicative rural topology even if respective critical measurement differences that may reach up to 10dB of measurement difference magnitude occur.
- Apart from curve similarity metric and topology identification tool, CSPM value warns about its accuracy degree. In fact, higher values of CSPM imply that: (i) topology identification becomes more precarious due to the rich multipath environment of the underlaid OV HV BPL topology; (ii) the spectral notches that are superimposed by the measurement differences on the coupling transfer functions become comparable with the inherent ones. In fact, CSPM values increase as the magnitude of measurement differences increases too in all the cases examined; (iii) even if the position of the underlaid OV HV BPL topology is first in ascending $CSPM_{\text{tot}}$ order among the other database topologies, the number of candidate topologies that are characterized by the same $CSPM_{\text{tot}}$ with the underlaid one increases; and (iv) the $CSPM_{\text{tot}}$ difference between the candidate OV HV BPL topologies of the set and the first topology outside the set decreases.
- The main component of TIM is its best L1PMA module. Based on the primary extrema, which are the main spectral notches, best L1PMA decomposes BPL transfer functions into separate monotonous sections between the primary extrema [1], [35], [36]. Since the number and the length of branches critically determine the number and the depth of spectral notches, the best L1PMA outputs of OV HV BPL topologies with the same branch number and length resemble each other regardless of the number of monotonic sections considered. This is verified by the same branch number and length that present the candidate OV HV BPL topologies of the set. Here, it is expected that the number of the candidate rural topologies is high since all the OV HV BPL topologies of one long branch resemble to the power divider behavior as described in Sec.VB.
- If the OV HV BPL topology is already known then the exact measurement differences can be computed on the basis of $CSPM_{\text{tot}}$ curves. Note that steep changes in the characteristics of the measurement difference distribution imply changes in the surrounding environment of OV HV BPL topologies.

Since the proposed TIM can identify an OV HV BPL topology even if measurement differences occur during the determination of its coupling transfer function, each OV HV BPL topology is almost uniquely characterized by the curve trend and the values of the $CSPM_{\text{tot}}$. Since two OV HV BPL topologies present different $CSPM_{\text{tot}}$ behavior, these topologies can be differentiated from each other. This implies that various serious faults and instabilities across the transmission power grid (e.g., line faults and line termination instabilities) can be first differentiated from the measurement differences and, then, be identified for given OV HV BPL topology. In the companion paper of [59], the proposed TIM is extended to the Fault and Instability Identification Methodology (FIIM) so that faults or instabilities across an intelligent energy system can be identified and the personnel, who is monitoring the transmission power grid, is warned so as to restore the power grid to default settings.

Conclusions

In this paper, the proposed TIM of an OV HV BPL topology, when a corresponding OV HV BPL coupling transfer function with measurement differences is available, has been presented. The TIM consists of: (i) the hybrid method; (ii) the best L1PMA; (iii) the proposed OV HV BPL topology database; and (iv) CSPM that serves as the assessment metric of the TIM accuracy.

As the validation of the TIM is concerned, the CSPM has achieved to reveal a set of candidate OV HV BPL topologies with the underlaid topology lying inside it even though measurement differences of various distributions and magnitudes have been applied.

In the companion paper of [59], TIM is extended to FIIM so that faults and instabilities across the OV HV BPL networks can be identified and the responsible personnel is warned.

Conflicts of Interest

The author declares that there is no conflict of interests regarding the publication of this paper.

References

[1] A. G. Lazaropoulos, "Best L1 Piecewise Monotonic Data Approximation in Overhead and Underground Medium-Voltage and Low-Voltage Broadband over Power Lines Networks: Theoretical and Practical Transfer Function Determination," *Hindawi Journal of Computational Engineering*, vol. 2016, Article ID 6762390, 24 pages, 2016. DOI: 10.1155/2016/6762390.

[2] C. Cano, A.Pittolo, D. Malone, L. Lampe, A. M.Tonello, and A. Dabak, "State-of-the-art in Power Line Communications: From the Applications to the Medium," *IEEE J. Sel. Areas Commun.*, vol. 34, pp. 1935-1952, 2016.

[3] A. Milioudis, G. Andreou, and D. Labridis, "Optimum transmitted power spectral distribution for broadband power line communication systems considering electromagnetic emissions," *Elsevier Electric Power Systems Research*, vol. 140, pp. 958–964, 2016. DOI: 10.1016/j.epsr.2016.03.047

[4] T. A. Papadopoulos, A. I. Chrysochos, E. O. Kontis, and G. K. Papagiannis, "Ringdown Analysis of Power Systems Using Vector Fitting," *Electric Power Systems Research*, vol. 141, pp. 100-103, 2016.

[5] A. G. Lazaropoulos, "Broadband transmission characteristics of overhead high-voltage power line communication channels," *Progress in Electromagnetics Research B*, vol. 36, pp. 373-398, 2012. [Online]. Available: http://www.jpier.org/PIERB/pierb36/19.11091408.pdf

[6] A. G. Lazaropoulos, "Broadband transmission and statistical performance properties of overhead high-voltage transmission networks," *Hindawi Journal of Computer Networks and Commun.*, 2012, article ID 875632, 2012. [Online]. Available: http://www.hindawi.com/journals/jcnc/aip/875632/

[7] A. G. Lazaropoulos, "Review and Progress towards the Common Broadband Management of High-Voltage Transmission Grids: Model Expansion and Comparative Modal Analysis," *ISRN Electronics*, vol. 2012, Article ID 935286,

pp. 1-18, 2012. [Online]. Available: http://www.hindawi.com/isrn/electronics/2012/935286/

[8] A. G. Lazaropoulos, "Capacity Performance of Overhead Transmission Multiple-Input Multiple-Output Broadband over Power Lines Networks: The Insidious Effect of Noise and the Role of Noise Models.," *Trends in Renewable Energy*, vol. 2, no. 2, pp. 61-82, Jan. 2016. DOI: 10.17737/tre.2016.2.2.0023

[9] A. I. Chrysochos, T. A. Papadopoulos, A. ElSamadouny, G. K. Papagiannis, and N. Al-Dhahir, "Optimized MIMO-OFDM design for narrowband-PLC applications in medium-voltage smart distribution grids," *Electric Power Systems Research*, vol. 140, pp. 253–262, 2016. DOI: 10.1016/j.epsr.2016.06.017

[10] A. G. Lazaropoulos and P. Lazaropoulos, "Financially Stimulating Local Economies by Exploiting Communities' Microgrids: Power Trading and Hybrid Techno-Economic (HTE) Model," *Trends in Renewable Energy*, vol. 1, no. 3, pp. 131-184, Sep. 2015. DOI: 10.17737/tre.2015.1.3.0014

[11] A. G. Lazaropoulos, "Wireless Sensor Network Design for Transmission Line Monitoring, Metering and Controlling: Introducing Broadband over PowerLines-enhanced Network Model (BPLeNM)," *ISRN Power Engineering*, vol. 2014, Article ID 894628, 22 pages, 2014. DOI:10.1155/2014/894628

[12] A. G. Lazaropoulos, "Wireless Sensors and Broadband over PowerLines Networks: The Performance of Broadband over PowerLines-enhanced Network Model (BPLeNM) (Invited Paper)," *ICAS Publishing Group Transaction on IoT and Cloud Computing*, vol. 2, no. 3, pp. 1-35, 2014. [Online]. Available: http://icas-pub.org/ojs/index.php/ticc/article/view/27/17

[13] S. S. Pappas, L. Ekonomou, D. C. Karamousantas, G. E. Chatzarakis, S. K. Katsikas, and P. Liatsis, "Electricity Demand Loads Modeling Using AutoRegressive Moving Average (ARMA) Models," Energy, vol. 33, no. 9, pp. 1353-1360, 2008. DOI: 10.1016/j.energy.2008.05.008

[14] A. G. Lazaropoulos and P. G. Cottis, "Transmission characteristics of overhead medium voltage power line communication channels," *IEEE Trans. Power Del.*, vol. 24, no. 3, pp. 1164-1173, Jul. 2009.

[15] A. G. Lazaropoulos and P. G. Cottis, "Capacity of overhead medium voltage power line communication channels," *IEEE Trans. Power Del.*, vol. 25, no. 2, pp. 723-733, Apr. 2010.

[16] A. G. Lazaropoulos and P. G. Cottis, "Broadband transmission via underground medium-voltage power lines-Part I: transmission characteristics," *IEEE Trans. Power Del.*, vol. 25, no. 4, pp. 2414-2424, Oct. 2010.

[17] A. G. Lazaropoulos and P. G. Cottis, "Broadband transmission via underground medium-voltage power lines-Part II: capacity," *IEEE Trans. Power Del.*, vol. 25, no. 4, pp. 2425-2434, Oct. 2010.

[18] F. Versolatto and A. M. Tonello, "An MTL theory approach for the simulation of MIMO power-line communication channels," *IEEE Trans. Power Del.*, vol. 26, no. 3, pp. 1710-1717, Jul. 2011.

[19] M. Zimmermann and K. Dostert, "Analysis and modeling of impulsive noise in broad-band powerline communications," *IEEE Trans. Electromagn. Compat.*, vol. 44, no. 1, pp. 249-258, Feb. 2002.

[20] A. G. Lazaropoulos, "Factors Influencing Broadband Transmission Characteristics of Underground Low-Voltage Distribution Networks," *IET Commun.*, vol. 6, no. 17, pp. 2886-2893, Nov. 2012.

[21] A. G. Lazaropoulos, "Towards broadband over power lines systems integration: Transmission characteristics of underground low-voltage distribution power lines," *Progress in Electromagnetics Research B*, 39, pp. 89-114, 2012. [Online]. Available: http://www.jpier.org/PIERB/pierb39/05.12012409.pdf

[22] A. G. Lazaropoulos, "Towards modal integration of overhead and underground low-voltage and medium-voltage power line communication channels in the smart grid landscape: model expansion, broadband signal transmission characteristics, and statistical performance metrics (Invited Paper)," *ISRN Signal Processing*, in press, [Online]. Available: http://www.isrn.com/journals/sp/aip/121628/

[23] A. G. Lazaropoulos, "Review and Progress towards the Capacity Boost of Overhead and Underground Medium-Voltage and Low-Voltage Broadband over Power Lines Networks: Cooperative Communications through Two- and Three-Hop Repeater Systems," *ISRN Electronics*, vol. 2013, Article ID 472190, pp. 1-19, 2013. [Online]. Available: http://www.hindawi.com/isrn/electronics/aip/472190/

[24] A. G. Lazaropoulos, "Green Overhead and Underground Multiple-Input Multiple-Output Medium Voltage Broadband over Power Lines Networks: Energy-Efficient Power Control," *Springer Journal of Global Optimization*, vol. 2012 / Print ISSN 0925-5001, pp. 1-28, Oct. 2012.

[25] P. Amirshahi and M. Kavehrad, "High-frequency characteristics of overhead multiconductor power lines for broadband communications," *IEEE J. Sel. Areas Commun.*, vol. 24, no. 7, pp. 1292-1303, Jul. 2006.

[26] T. Sartenaer, "Multiuser communications over frequency selective wired channels and applications to the powerline access network" Ph.D. dissertation, Univ. Catholique Louvain, Louvain-la-Neuve, Belgium, Sep. 2004.

[27] T. Calliacoudas and F. Issa, ""Multiconductor transmission lines and cables solver," An efficient simulation tool for plc channel networks development," presented at the *IEEE Int. Conf. Power Line Communications and Its Applications*, Athens, Greece, Mar. 2002.

[28] A. G. Lazaropoulos, "Policies for Carbon Energy Footprint Reduction of Overhead Multiple-Input Multiple-Output High Voltage Broadband over Power Lines Networks," *Trends in Renewable Energy*, vol. 1, no. 2, pp. 87-118, Jun. 2015. DOI: 10.17737/tre.2015.1.2.0011

[29] T. Sartenaer and P. Delogne, "Deterministic modelling of the (Shielded) outdoor powerline channel based on the multiconductor transmission line equations," *IEEE J. Sel. Areas Commun.*, vol. 24, no. 7, pp. 1277-1291, Jul. 2006.

[30] C. R. Paul, *Analysis of Multiconductor Transmission Lines*. New York: Wiley, 1994.

[31] T. A. Papadopoulos, A. I. Chrysochos, and G. K. Papagiannis, "Narrowband Power Line Communication:Medium Voltage Cable Modeling and Laboratory Experimental Results,"*Electric Power Systems Research*, vol. 102, pp. 50-60, 2013.

[32] A. N. Milioudis, G. T. Andreou, and D. P. Labridis, "Enhanced Protection Scheme for Smart Grids Using Power Line Communications Techniques—Part II: Location ofHigh Impedance Fault Position," *IEEE Trans. on Smart Grid*, no. 3, vol. 4, pp. 1631-1640, 2012.

[33] I. C. Demetriou and M. J. D. Powell, "Least squares smoothing of univariate data to achieve piecewise monotonicity," *IMA J. of Numerical Analysis*, vol. 11, pp. 411-432, 1991.

[34] I. C. Demetriou and V. Koutoulidis"On Signal Restoration by Piecewise Monotonic Approximation", in Lecture Notes in Engineering and Computer Science: *Proceedings of The World Congress on Engineering 2013*,London, U.K., Jul. 2013, pp. 268-273.

[35] I. C. Demetriou, "An application of best *L*1 piecewise monotonic data approximation to signal restoration," *IAENG International Journal of Applied Mathematics*, vol. 53, no. 4, pp. 226-232, 2013.

[36] I. C. Demetriou, "L1PMA: A Fortran 77 Package for Best L1 Piecewise Monotonic Data Smoothing," *Computer Physics Communications*, vol. 151, no. 1, pp. 315-338, 2003.

[37] I. C. Demetriou, "Data Smoothing by Piecewise Monotonic Divided Differences," *Ph.D. Dissertation*, Department of Applied Mathematics and Theoretical Physics, University of Cambridge, Cambridge, 1985.

[38] I. C. Demetriou, "Best L1 Piecewise Monotonic Data Modelling,"*Int. Trans. Opl Res.*, vol. 1, no. 1, pp. 85-94,1994.

[39] I.C. Demetriou, "L1PMA: a Fortran 77 package for best L1 piecewise monotonic data smoothing," 2003 http://cpc.cs.qub.ac.uk/summaries/ADRF

[40] P. Amirshahi, "Broadband access and home networking through powerline networks" Ph.D. dissertation, Pennsylvania State Univ., University Park, PA, May 2006. [Online]. Available: http://etda.libraries.psu.edu/theses/approved/WorldWideIndex/ETD-1205/index.html

[41] N. Suljanović, A. Mujčić, M. Zajc, and J. F. Tasič, "Approximate computation of high-frequency characteristics for power line with horizontal disposition and middle-phase to ground coupling," *Elsevier Electr. Power Syst. Res.*, vol. 69, pp. 17-24, Jan. 2004.

[42] M. D'Amore and M. S. Sarto, "Simulation models of a dissipative transmission line above a lossy ground for a wide-frequency range-Part I: Single conductor configuration," *IEEE Trans. Electromagn. Compat.*, vol. 38, no. 2, pp. 127-138, May 1996.

[43] M. D'Amore and M. S. Sarto, "Simulation models of a dissipative transmission line above a lossy ground for a wide-frequency range-Part II: Multi-conductor configuration," *IEEE Trans. Electromagn. Compat.*, vol. 38, no. 2, pp. 139-149, May 1996.

[44] A. G. Lazaropoulos, "The Impact of Noise Models on Capacity Performance of Distribution Broadband over Power Lines (BPL) Networks," *Hindawi Computer Networks and Communications*, vol. 2016, Article ID 5680850, 14 pages, 2016. doi:10.1155/2016/5680850. [Online]. Available: http://www.hindawi.com/journals/jcnc/2016/5680850/

[45] A. G. Lazaropoulos, "Designing Broadband over Power Lines Networks Using the Techno-Economic Pedagogical (TEP) Method – Part I: Overhead High Voltage Networks and Their Capacity Characteristics," *Trends in Renewable Energy*, vol. 1, no. 1, pp. 16-42, Mar. 2015. DOI: 10.17737/tre.2015.1.1.002

[46] OPERA1, D5: Pathloss as a function of frequency, distance and network topology for various LV and MV European powerline networks. IST Integrated Project No 507667, Apr. 2005.

[47] OPERA1, D44: Report presenting the architecture of plc system, the electricity network topologies, the operating modes and the equipment over which PLC access system will be installed, IST Integr. Project No 507667, Dec. 2005.
[48] R. Pighi and R. Raheli, "On Multicarrier Signal Transmission for High-Voltage Power Lines," in *Proc. IEEE Int. Symp. Power Line Commun. Appl.*, Vancouver, BC, Canada, Apr. 2005, pp. 32-36.
[49] C. de Boor, *A Practical Guide to Splines*. Revised Edition, NY: Springer-Verlag, Applied Mathematical Sciences, vol. 27, 2001.
[50] M. Holschneider, *Wavelets. An Analysis Tool*, Oxford: Clarendon Press, 1997.
[51] M. J. D. Powell, *Approximation Theory and Methods*. Cambridge, U.K.: Cambridge University Press, 1981.
[52] A. G. Lazaropoulos, *Engineering the Art through the Lens of L1PMA: A Tribute to the Modern Greek Painters*, Art Book ISSUU Digital Publishing Platform, Oct. 2014. [Online]. Available: http://issuu.com/lazaropoulos/docs/l1pma
[53] A. G. Lazaropoulos, *ReEngineering the Art through the Lens of L2WPMA: A Tribute to Leonardo da Vinci'sInventions: Flying Machines, War Machines, Architect/Innovations and Water Land Machines*, Art Book ISSUU Digital Publishing Platform, Nov. 2014. [Online]. Available: http://issuu.com/lazaropoulos/docs/l2wpma
[54] A. G. Lazaropoulos, *ReEngineering the Art through the Lens of L1PMA L2WPMA: The Eternal Youth ofthe Parthenon Art, Architecture, Marble Sculpture, Metallurgy Pottery*, Art Book ISSUU Digital Publishing Platform, Dec. 2014. [Online]. Available: http://issuu.com/lazaropoulos/docs/l1pma_l2wpma
[55] T. Banwell and S. Galli, "A novel approach to accurate modeling of the indoor power line channel—Part I: Circuit analysis and companion model," *IEEE Trans. Power Del.*, vol. 20, no. 2, pp. 655-663, Apr. 2005.
[56] S. Galli and T. Banwell, "A novel approach to accurate modeling of the indoor power line channel — Part II: Transfer function and channel properties," *IEEE Trans. Power Del.*, vol. 20, no. 3, pp. 1869-1878, Jul. 2005.
[57] S. Galli and T. Banwell, "A deterministic frequency-domain model for the indoor power line transfer function," *IEEE J. Sel. Areas Commun.*, vol. 24, no. 7, pp. 1304-1316, Jul. 2006.
[58] A. G. Lazaropoulos, "Deployment Concepts for Overhead High Voltage Broadband over Power Lines Connections with Two-Hop Repeater System: Capacity Countermeasures against Aggravated Topologies and High Noise Environments," *Progress in Electromagnetics Research B*, vol. 44, pp. 283-307, 2012. [Online]. Available: http://www.jpier.org/PIERB/pierb44/13.12081104.pdf
[59] A. G. Lazaropoulos, "Measurement Differences, Faults and Instabilities in Intelligent Energy Systems – Part 2: Fault and Instability Prediction in Overhead High-Voltage Broadband over Power Lines Networks by Applying Fault and Instability Identification Methodology (FIIM)," *Trends in Renewable Energy*, 2(3), 113-142. DOI: 10.17737/tre.2016.2.3.0027

Trends in Renewable Energy
OPEN ACCESS ISSN:2376-2144
Peer-Reviewed Article futureenergysp.com/index.php/tre

Measurement Differences, Faults and Instabilities in Intelligent Energy Systems – Part 2: Fault and Instability Prediction in Overhead High-Voltage Broadband over Power Lines Networks by Applying Fault and Instability Identification Methodology (FIIM)

Athanasios G. Lazaropoulos[1]

1: School of Electrical and Computer Engineering, National Technical University of Athens, 9 IroonPolytechniou Street, Zografou, GR 15780 Greece

Received August 26, 2016; Accepted September 23, 2016; Published October 3, 2016

This companion paper of [1] focuses on the prediction of various faults and instabilities that may occur during the operation of the transmission power grid when overhead high-voltage broadband over power lines (OV HV BPL) networks are deployed across it. Having already been identified the theoretical OV HV BPL transfer function for a given OV HV BPL network [1], the faults and instabilities of the transmission power grid are first differentiated from the measurement differences, which can occur during the determination of an OV HV BPL transfer function, and, then, are identified by applying the best L1 Piecewise Monotonic data Approximation (best L1PMA) to the measured OV HV BPL transfer function. When faults and instabilities are detected, a warning is issued.
The contribution of this paper is triple. First, the Topology Identification Methodology (TIM) of [1] is here extended to the proposed Fault and Instability Identification Methodology (FIIM) so that faults and instabilities across the transmission power grid can be identified. Also, the curve similarity performance percentage metric (CSPpM) that acts as the accompanying performance metric of FIIM is introduced. Second, the impact of various fault and instability conditions on the OV HV BPL transfer functions is demonstrated. Third, the fault and instability prediction procedure by applying the FIIM is first reported.

Keywords: Smart Grid; Intelligent Energy Systems; Broadband over Power Lines (BPL) networks; Power Line Communications (PLC); Faults; Fault Analysis; Transmission Power Grids

1. Introduction

The deployment of broadband over power lines (BPL) networks across the vintage overhead high-voltage (OV HV) power grid can transform it into a modern IP-based communications network with a great number of smart grid applications [1]. Among the available smart grid applications, this companion paper focuses on the transmission power grid protection that is a critical matter for both operational and safety reasons [2]-[5].

Corresponding author: AGLazaropoulos@gmail.com

Tr Ren Energy, 2016, Vol.2, No.3, 113-142. doi: 10.17737/tre.2016.2.3.0027

In fact, the development of an efficient protection scheme, which can ensure the adequate operation of the power grid as well as the protection of its equipment, has attracted the academic interest for many years. The protection scheme proposals have mainly been based on traditional circuit analysis solutions [6], artificial intelligence methods [7]-[10], wavelet transformations [11]-[15] and narrowband power line communications applications [12], [13], [16]. Only recently, the broadband potential of power grid has been recognized and exploited as a formidable basis on which the protection capability of the power grid is further enhanced [2], [17]-[21].

In this companion paper, the Fault and Instability Identification Methodology (FIIM) is proposed that exploits the well-validated knowledge concerning: (i) the BPL network operation across transmission and distribution power grids (i.e., hybrid method of [22]-[36]); (ii) the anti-fault operation of best L1PMA [1], [37]; and (iii) the Topology Identification Methodology (TIM) of [1]. More analytically, a number of practical reasons and "real-life" conditions may create measurement differences between experimental and theoretical results during the transfer function determination of OV HV BPL networks. By adopting best L1PMA, which is theoretically presented and experimentally verified in various systems including transmission and distribution BPL networks [1], [37]-[44], an OV HV BPL network topology can be identified despite the fact that measurement differences occur during the determination of its measured OV HV BPL transfer function. However, various serious faults and instabilities can occur across the transmission power grid and create significant fault conditions whose nature differ from the aforementioned "innocent" measurement differences (e.g., line faults and instabilities). By applying FIIM, these fault conditions are first differentiated from the measurement differences and then are identified. In fact, the contribution of the FIIM in comparison with the traditional one is that it can surely identify fault and instability conditions without creating a fault alarm situation despite the fact that measurement differences occur. From the moment that a fault or instability is identified, the personnel, who is monitoring the transmission power grid, is warned so as to restore the power grid to default settings.

The rest of this companion paper is organized as follows: In Sec. II, the faults and instabilities, which are examined in this paper, are detailed with reference to indicative topologies and the hybrid-method. In Sec. III, a presentation of the FIIM and its appropriate curve similarity performance percentage metric (CSPpM) are given. Sec.IV discusses the simulations of various transmission BPL networks intending to mark out the efficiency of FIIM to issue warnings due to serious faults and instabilities of the transmission intelligent energy system. Sec.V concludes this paper.

2. Faults and Instabilities in Transmission Power Grids

2.1 Indicative OV HV BPL Topologies

In accordance with [1], [22]-[35], [45]-[48] and with reference to Fig. 1(a), average path lengths of the order of 25km are considered in OV HV BPL topologies. Apart from the three indicative OV HV BPL topologies of [1], another one that describes the OV HV BPL signal propagation and transmission in more aggravated environments such those of urban areas is added. Hence, the following four indicative OV HV BPL topologies, concerning end-to-end connections of average path lengths, are examined, as follows:

1. A typical urban topology (OV HV urban case) with N=3 branches (L_1=1km, L_2=12km, L_3=8km, L_4=4km, L_{b1}=24km, L_{b2}=2km, L_{b3}=7km).
2. A typical suburban topology (OV HV suburban case) with N=2 branches (L_1=9km, L_2=13km, L_3=3km, L_{b1}=17km, L_{b2}=13km).
3. A typical rural topology (OV HV rural case) with only N=1 branch (L_1=4km, L_2=21km, L_{b1}=24km).
4. The "LOS" transmission along the same end-to-end distance $L=L_1+\ldots+L_{N+1}$=25km when no branches are encountered. This topology corresponds to Line of Sight transmission in wireless channels.

The four indicative OV HV BPL topologies are going to be used so that the accuracy of the proposed FIIM is evaluated in Sec.IV.

The assumptions for the circuital parameters of OV HV BPL topologies, which are concerned in this companion paper, are the same with [1], namely: (i) The branch lines are assumed identical to the transmission lines; (ii) The interconnections between the transmission and branch conductors of the lines are fully activated; (iii) The transmitting and the receiving ends are assumed matched to the characteristic impedance of the modal channels; and (iv) The branch terminations are assumed to be open circuits.

2.2 Modeling of Faults and Instabilities in OV HV BPL Topologies

As already been mentioned in [1], a set of practical reasons and "real-life" conditions can create significant differences between measurements and theoretical results during the transfer function determination of BPL networks. The reasons for these measurement differences have been grouped into six categories [1], [37], [49]-[51]. According to [1], [37], the total occurred fault due to the six measurement difference categories can be assumed to follow either continuous uniform distribution (CUD) with minimum value $-a_{CUD}$ and maximum value a_{CUD} or normal distribution (ND) with mean m_{ND} and standard deviation s_{ND}.

Apart from the aforementioned "innocent" measurement differences, which can be anyway satisfactorily mitigated by the TIM of [1], various serious problematic conditions across the transmission power grid can occur whose nature differs from this of the aforementioned measurement differences. In fact, these problematic conditions cause permanent damage to the transmission power grid, do not follow any error distribution and their impact on the determination of OV HV BPL transfer functions totally change the form of the result. In this paper, the problematic conditions are divided into two categories, namely:

Trends in Renewable Energy
OPEN ACCESS ISSN:2376-2144

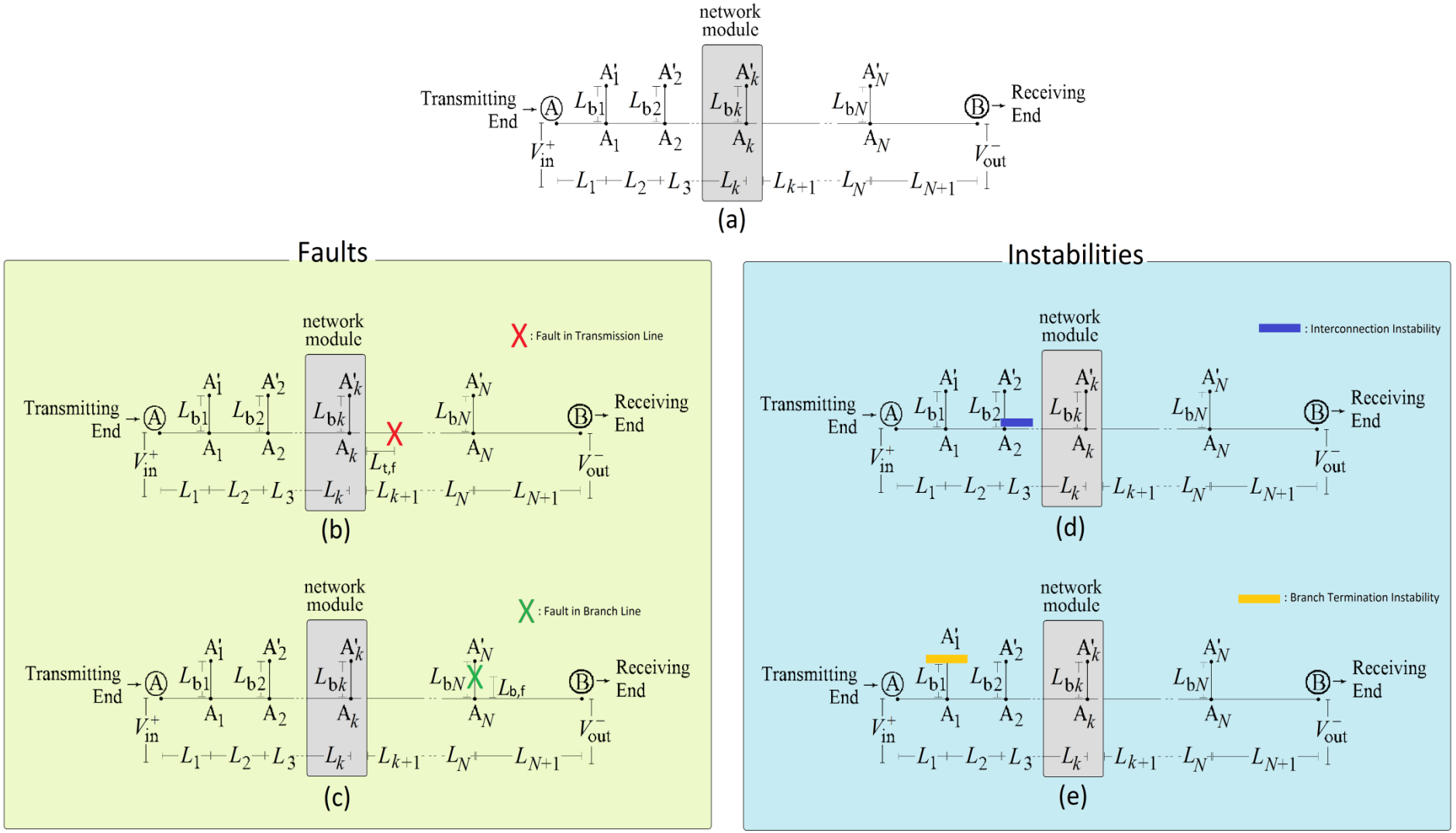

Figure 1. (a) General OV HV BPL topology [1]. (b, c) Faults in OV HV BPL topologies. (d, e) Instabilities in OV HV BPL topologies.

*Corresponding author: AGLazaropoulos@gmail.com

Tr Ren Energy, 2016, Vol.2, No.3, 113-142. doi: 10.17737/tre.2016.2.3.0027

- *Faults*: This category describes all the interruptions that can occur in the lines of a transmission power grid. There are two subcategories of line interruptions that are examined in this paper:
  - *Fault in Transmission Line*: This fault subcategory describes the condition where a transmission line is interrupted due to physical or human reasons. With reference to Fig. 1(b), let the transmission line be broken at the position $\sum_{i=1}^{k} L_k + L_{\mathrm{t,f}}$ from the transmitting end. This incident has as a result the communications failure between the transmitting and receiving end. Since all the other BPL network settings are well-verified, the personnel that is responsible for the transmission power grid operation is immediately warned by the FIIM with the reason of a fault in transmission line. The methodology of the exact fault position has already been presented in [2], [17]-[20]. Anyway, the localization of the faults and instabilities is outside of the scope of this paper and is not analyzed further.
  - *Fault in Branch Line*: Similarly to faults in transmission lines, this fault subcategory describes the condition where a branch line is interrupted. With reference to Fig. 1(c), let the branch N be broken at the position $L_{\mathrm{b,f}}$ from the branching interconnection A_N with the transmission line. In contrast with faults in transmission lines, this problematic condition does not critically influence the communication between the transmitting and receiving end, nevertheless, it may create permanent undetectable failure and severely degrade the BPL network performance. However, the interruption of the N branch (i.e., open circuit) transfers the termination from $L_{\mathrm{b}N}$ to $L_{\mathrm{b,f}}$, thus, converting the examined N-branch OV HV BPL topology into a new N-branch OV HV BPL topology. Even if measurement differences occur, FIIM recognizes this fault condition and warns the responsible personnel. Simulation results concerning faults in branch lines and their identification by FIIM are presented in Sec.IVD.
- *Instabilities*: This category describes all the failures that can occur in the equipment across the transmission power grid. There are two subcategories of equipment failures that are examined in this paper:
  - *Instability in Branch Interconnections*: One assumption of the hybrid method definition is that the interconnections between the transmission and branch lines are fully activated. However, these connectors may present faults having as a result the partial or total interruption of the branch line. With reference to Fig. 1(d), the total interruption of the second branch at the point A_2 cancels the presence of this branch, thus, converting the examined N-branch OV HV BPL topology into a (N-1)-branch OV HV BPL topology. Depending on the termination of this branch (i.e., transformer HV/MV, load or source), significant instability during the operation of the transmission power grid can occur. FIIM can recognize this instability condition and warn the responsible personnel. Simulation results concerning instabilities in branch interconnections and their identification by FIIM are presented in Sec.IVE.

*Corresponding author: AGLazaropoulos@gmail.com

Tr Ren Energy, 2016, Vol.2, No.3, 113-142. doi: 10.17737/tre.2016.2.3.0027

- *Instability in Branch Terminations*: Again, one assumption of the fine hybrid method operation is that the branch terminations are assumed to be open circuits. This is due to the fact that HV/MV transformers are connected to the branch terminations, which are treated as open circuit terminations when high-frequency signals are considered. Physical stress on transformer windings, overloads, thermal aging of winding insulation, mechanical shake of windings and overflow or tank rupture are among the main causes of faults in HV/MV transformers. Since HV/MV transformers are critical pieces of equipment during the operation of power systems, their failure can create significant instabilities during their operation. With reference to Fig. 1(e), let the branch termination of first branch stop to act as open circuit termination. In that case, the branch termination fluctuates and so does the performance of transmission power grid. Again, FIIM can recognize this instability condition and warn the responsible personnel. Simulation results concerning instabilities in branch terminations and their identification by FIIM are presented in Sec.IVF.

3. FIIM and CSPpM

3.1 Implementation Details

In accordance with [1], a set of practical reasons and "real-life" conditions create significant differences between experimental measurements and theoretical results during the transfer function determination of BPL networks. The reasons for these measurement differences have been grouped into six categories. Then, the measured OV HV coupling transfer function $\overline{H^{\mathrm{WtG}}\{\cdot\}}$ is determined by

$$\overline{H^{\mathrm{WtG}}}(f_i) = H^{\mathrm{WtG}}(f_i) + e(f_i) \tag{1}$$

where f_i denotes the measurement frequency, $H^{\mathrm{WtG}}\{\cdot\}$ is the theoretical OV HV coupling transfer function and $e(f_i)$ synopsizes the total measurement difference due to the aforementioned six categories. The measurement frequencies f_i, i=1,…,u, the measured OV HV coupling transfer functions $\overline{H^{\mathrm{WtG}}}(f_i)$, i=1,…,u and the theoretical OV HV coupling transfer functions $H^{\mathrm{WtG}}(f_i)$, i=1,…,u can be treated as elements of $\mathbf{f}$, $\overline{\mathbf{H}^{\mathrm{WtG}}}$ and $\mathbf{H}^{\mathrm{WtG}}$, respectively, where

$$\mathbf{f} = \begin{bmatrix} f_1 & \cdots & f_i & \cdots & f_u \end{bmatrix}^{\mathrm{T}},\ i=1,\ldots,u \tag{2}$$

$$\overline{\mathbf{H}^{\mathrm{WtG}}} \equiv \overline{\mathbf{H}^{\mathrm{WtG}}}(\mathbf{f}) = \begin{bmatrix} \overline{H^{\mathrm{WtG}}}(f_1) & \cdots & \overline{H^{\mathrm{WtG}}}(f_i) & \cdots & \overline{H^{\mathrm{WtG}}}(f_u) \end{bmatrix}^{\mathrm{T}},\ i=1,\ldots,u \tag{3}$$

$$\mathbf{H}^{\mathrm{WtG}} \equiv \mathbf{H}^{\mathrm{WtG}}(\mathbf{f}) = \begin{bmatrix} H^{\mathrm{WtG}}(f_1) & \cdots & H^{\mathrm{WtG}}(f_i) & \cdots & H^{\mathrm{WtG}}(f_u) \end{bmatrix}^{\mathrm{T}},\ i=1,\ldots,u \tag{4}$$

As the application of best L1PMA is concerned, best L1PMA and its corresponding curve similarity performance metric (CSPM) achieve to reveal the OV HV BPL topology even though measurement differences of various distributions and magnitudes have been applied [1]. In this paper, each indicative OV HV BPL topology of Sec.IIA is accompanied with a number of approximated measured OV HV BPL coupling transfer function column vector $\overline{\overline{\mathbf{H}^{\mathrm{WtG}}_{\mathrm{meas}}}}(\mathbf{f}, k_{\mathrm{sect}})$ and approximated theoretical OV HV BPL

coupling transfer function column vector $\overline{\overline{\mathbf{H}_{\text{theor}}^{\text{WtG}}}}\left(\mathbf{f},k_{\text{sect}}\right)$ that come from the application of the best L1PMA for different monotonic sections k_{sect}. Note that monotonic sections may range from 1 to $k_{\text{sect,max}}$ where $k_{\text{sect,max}}$ is the maximum number of monotonic sections considered in this paper. Hence, for each indicative OV HV BPL topology, the total $CSPM_{\text{tot}}$ is determined from

$$CSPM_{\text{tot}} \equiv \sum_{k_{\text{sect}}=1}^{k_{\text{sect,max}}} CSPM_{k_{\text{sec}\,t}} \tag{5}$$

where

$$CSPM_{k_{\text{sec}\,t}} \equiv CSPM_{k_{\text{sec}\,t}}\left(\overline{\mathbf{H}^{\text{WtG}}},\mathbf{H}^{\text{WtG}},k_{\text{sect}}\right)=\sum_{i=1}^{u}\left|\overline{\overline{\mathbf{H}_{\text{meas}}^{\text{WtG}}}}\left(f_i,k_{\text{sect}}\right)-\overline{\overline{\mathbf{H}_{\text{theor}}^{\text{WtG}}}}\left(f_i,k_{\text{sect}}\right)\right| \tag{6}$$

denotes the sum of the absolute errors between the best L1PMA measurement approximation and best L1PMA theory approximation for given monotonic section.

On the basis of eq.(5) and eq.(6), the proposed curve similarity performance percentage metric (CSPpM), which acts as the accompanying performance metric of FIIM, is here determined from

$$CSPpM \equiv 100\% \cdot \frac{\sum_{k_{\text{sect}}=1}^{k_{\text{sect,max}}}\sum_{i=1}^{u}\frac{\left|\overline{\overline{\mathbf{H}_{\text{meas}}^{\text{WtG}}}}\left(f_i,k_{\text{sect}}\right)-\overline{\overline{\mathbf{H}_{\text{theor}}^{\text{WtG}}}}\left(f_i,k_{\text{sect}}\right)\right|}{\left|\overline{\overline{\mathbf{H}_{\text{theor}}^{\text{WtG}}}}\left(f_i,k_{\text{sect}}\right)\right|}}{k_{\text{sect,max}}\times u} \tag{7}$$

Actually, CSPpM is a percentage metric that presents a specific pattern for an OV HV BPL topology. Hence, on the basis of TIM of [1], CSPpM may easily be retrieved during the normal operation of the transmission power grid for given OV HV BPL topology. As it is verified in Sec.IVB, this pattern stability allows CSPpM to act as health metric for an OV HV BPL topology.

In accordance with Sec.IIB, if a fault or instability occurs across the examined original OV HV BPL topology then a modified OV HV BPL topology should be examined. In that case, the measured OV HV coupling transfer function $\overline{H^{\text{WtG*}}}\{\cdot\}$ of the modified topology is determined by

$$\overline{H^{\text{WtG*}}}\left(f_i\right)=H^{\text{WtG*}}\left(f_i\right)+e^{*}\left(f_i\right) \tag{8}$$

where $H^{\text{WtG*}}\{\cdot\}$ is the theoretical OV HV coupling transfer function of the modified topology and $e^{*}(f_i)$ synopsizes the new total measurement difference due to the aforementioned six categories. Similarly to the original OV HV BPL topology, the CSPpM of the modified OV HV BPL topology is given from

$$CSPpM^{*} \equiv 100\% \cdot \frac{\sum_{k_{\text{sect}}=1}^{k_{\text{sect,max}}}\sum_{i=1}^{u}\frac{\left|\overline{\overline{\mathbf{H}_{\text{meas}}^{\text{WtG*}}}}\left(f_i,k_{\text{sect}}\right)-\overline{\overline{\mathbf{H}_{\text{theor}}^{\text{WtG}}}}\left(f_i,k_{\text{sect}}\right)\right|}{\left|\overline{\overline{\mathbf{H}_{\text{theor}}^{\text{WtG}}}}\left(f_i,k_{\text{sect}}\right)\right|}}{k_{\text{sect,max}}\times u} \tag{9}$$

where $\overline{\overline{\mathbf{H}_{\text{meas}}^{\text{WtG*}}}}\left(\mathbf{f},k_{\text{sect}}\right)$ is the approximated measured OV HV BPL coupling transfer function column vector of the modified topology that comes from the application of the best L1PMA for different monotonic sections k_{sect}. Here, it should be noted that as the

original OV HV BPL topology is already known via [1], so does its theoretical OV HV BPL coupling transfer function as well as its best L1PMA approximation.

Based on eq. (7) and eq. (9), FIIM can recognize either fault or instability that may occur across the transmission power grid and warn the responsible personnel. Actually, FIIM first computes the CSPpM difference between the original OV HV BPL topology and the modified one that is given by

$$\Delta CSPpM^{*} = CSPpM \; - CSPpM^{*} \tag{10}$$

Then, FIIM compares $\Delta CSPpM^{*}$ with a warning threshold $\Delta CSPpM_{\text{thr}}^{*}$. Details concerning the determination of the warning threshold $\Delta CSPpM_{\text{thr}}^{*}$ and the relative decisions are provided in SecIVD-F.

3.2 Traditional FIIM

The traditional FIIM is mainly based on the observation and the experience of the responsible personnel. When greater differences of the usual case of measured OV HV coupling transfer function are observed then a warning is issued. However, the traditional FIIM is significantly unreliable due to the fact that a temporal or continuous concatenation of significant measurement differences (e.g., physical phenomena, random events) may wrongfully trigger the alarm.

In mathematical terms, traditional FIIM can be approximated by a methodology less sophisticated than the proposed FIIM one. Indeed, the percentage error sum (PES) that is given from

$$PES^{*} \equiv 100\% \cdot \frac{\sum_{i=1}^{u} \frac{\left|\mathbf{H}_{\text{meas}}^{\text{WtG*}}(f_i) - \mathbf{H}_{\text{meas}}^{\text{WtG}}(f_i)\right|}{\left|\mathbf{H}_{\text{meas}}^{\text{WtG}}(f_i)\right|}}{u} \tag{11}$$

is compared against an empirical warning threshold PES_{thr}^{*} that is typically equal to zero (risky decisions). If PES^{*} is greater or equal than PES_{thr}^{*}, a warning message is sent to the responsible personnel. As already been mentioned, this warning threshold primarily depends on the experience of the personnel and the employee's individuality.

4. Numerical Results and Discussion

4.1 Simulation Goals and Parameters

Various types of transmission BPL networks are simulated with the purpose of evaluating the proposed FIIM against the traditional one. Similarly to the TIM of [1], the efficiency of the FIIM is assessed with regards to the transmission BPL topologies and the nature of measurement differences.

As regards the hybrid method and best L1PMA specifications, those are the same with [1]. More specifically, the BPL frequency range and the flat-fading subchannel frequency spacing are assumed equal to 1-30MHz and 1MHz, respectively. Therefore, the number of subchannels u in the examined frequency range is equal to 30. Arbitrarily, the WtG^3 coupling scheme is applied during the following simulations. Finally, the maximum number of monotonic sections $k_{\text{sect,max}}$ that is going to be used is assumed to be equal to 20 [37].

4.2 CSPM, CSPpM and Indicative OV HV BPL Topologies

As already been reported in [1], [37] and Sec.IIIA, there are six categories that can create significant measurement differences between measurements and theoretical results during the determination of OV HV BPL coupling transfer functions. The total occurred fault due to the six measurement difference categories, which is described in eq. (1) and eq. (8), can be assumed to follow either CUD with minimum value $-a_{CUD}$ and maximum value a_{CUD} or normal distribution ND with mean m_{ND} and standard deviation s_{ND}.

With reference to eq. (7), *CSPpM* is based on the $CSPM_{tot}$ of TIM [1] and acts as the accompanying performance metric of FIIM. In Fig. 2(a), the $CSPM_{tot}$ of the indicative urban, suburban, rural and "LOS" topologies is plotted versus the CUD maximum value of the occurred measurement differences. Similar curves with Fig. 2(a) are given in Fig. 2(b) but for different values of ND standard deviation when m_{ND} is equal to 0dB. In Figs. 3(a) and 3(b), the same plots are given with Figs. 2(a) and 2(d) but for the *CSPpM*.

From Fig. 2(a), 2(b), 3(a) and 3(b), it is evident that:

- CSPM and CSPpM are generally increasing functions of CUD maximum value or ND standard deviation regardless of the OV HV BPL topology examined. Since both CSPM and CSPpM describe the integrity of OV HV BPL coupling transfer functions, as the measurement difference magnitudes increase so does the diversity of transfer functions.
- Although CSPM and CSPpM are both increasing functions of CUD maximum value or ND standard deviation, their behavior with respect to the multipath environment intensity changes. For given CUD maximum value or ND standard deviation, as the multipath environment becomes richer, CSPM curves increase whereas CSPpM curves decrease. Say, CSPM curves of "LOS" topology generally lay on bottom whereas the respective CSPpM ones lay on top.
- The smoothness trend of CSPM and CSPpM curves (i.e., the transition from zero to a maximum value), the maximum value of the curves and the curve notches act as an identity pattern for given OV HV BPL topology. This property of CSPM and CSPpM curves is exploited by the FIIM in order to distinguish the faults and instabilities from the measurement differences.
- The same CPSM and CSPpM conclusions can be deduced regardless of the measurement difference distribution applied (i.e, either CUD or ND).

In the following subsections, the FIIM performance is examined against the faults, instabilities and measurement differences. The proposed FIIM efficiency is compared against the traditional FIIM efficiency. Note that since the faults and instabilities that are examined in this paper has to do with branches, branch terminations and branch interconnections with the transmission lines, "LOS" topology is not further examined. Also, since the results concerning the performance of CSPM and CSPpM are almost the same and for the sake of simplicity and manuscript size, only one of the previous measurement difference distributions (e.g., CUD) will be applied, hereafter.

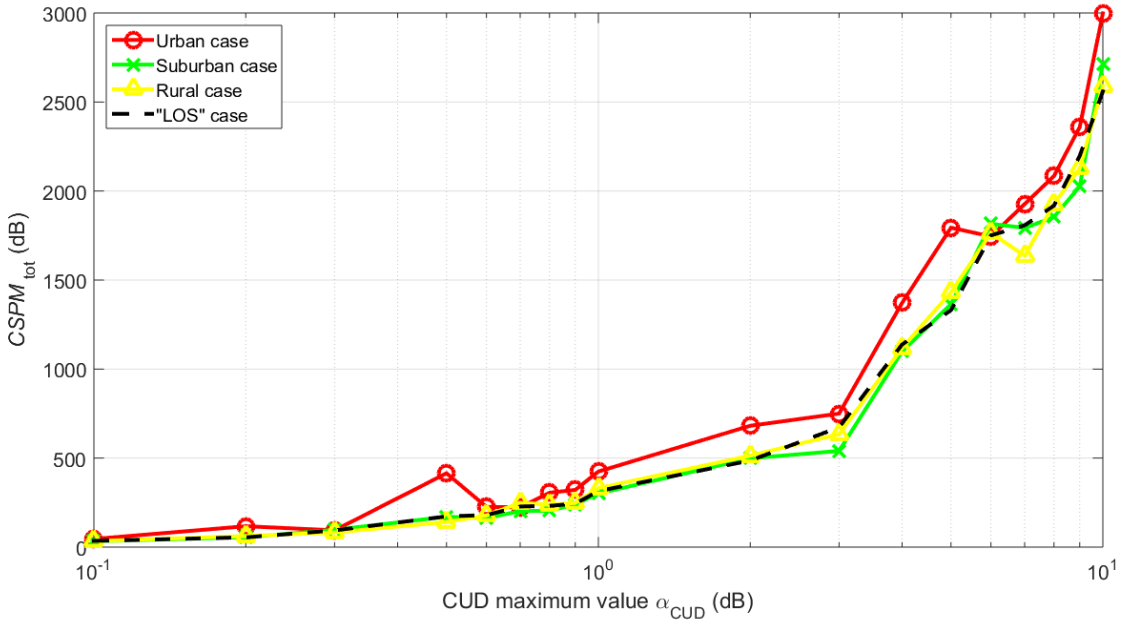

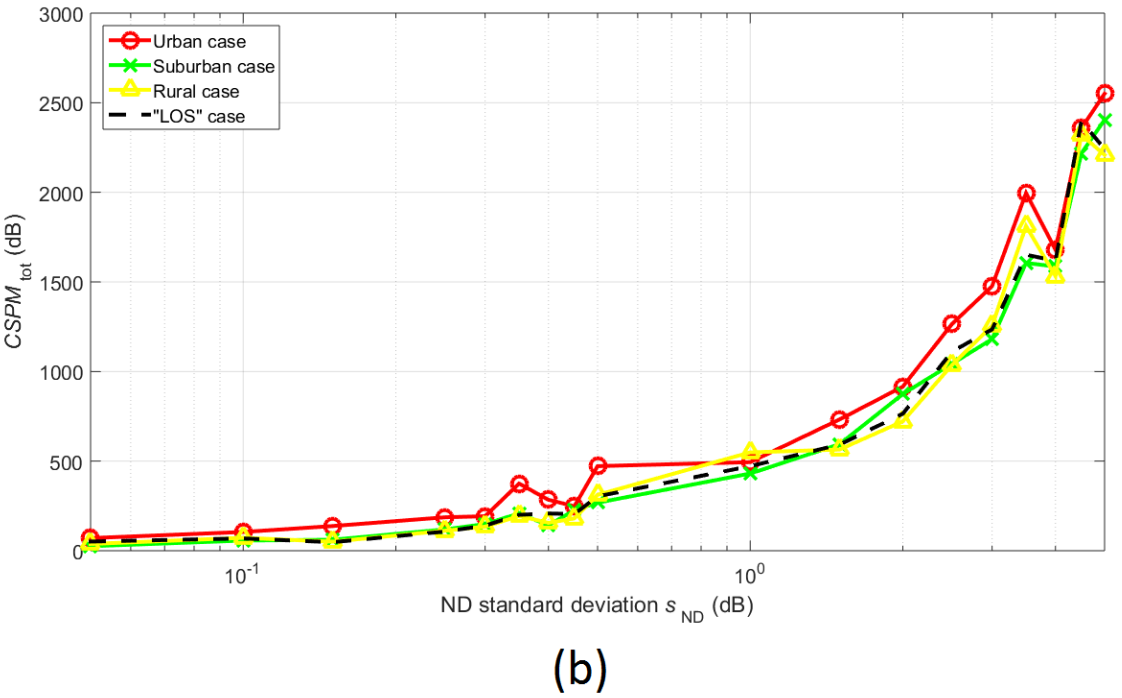

Figure 2. (a) $CSPM_{tot}$ versus CUD maximum value for the indicative OV HV BPL topologies. (b) $CSPM_{tot}$ versus ND standard deviation for the indicative OV HV BPL topologies.

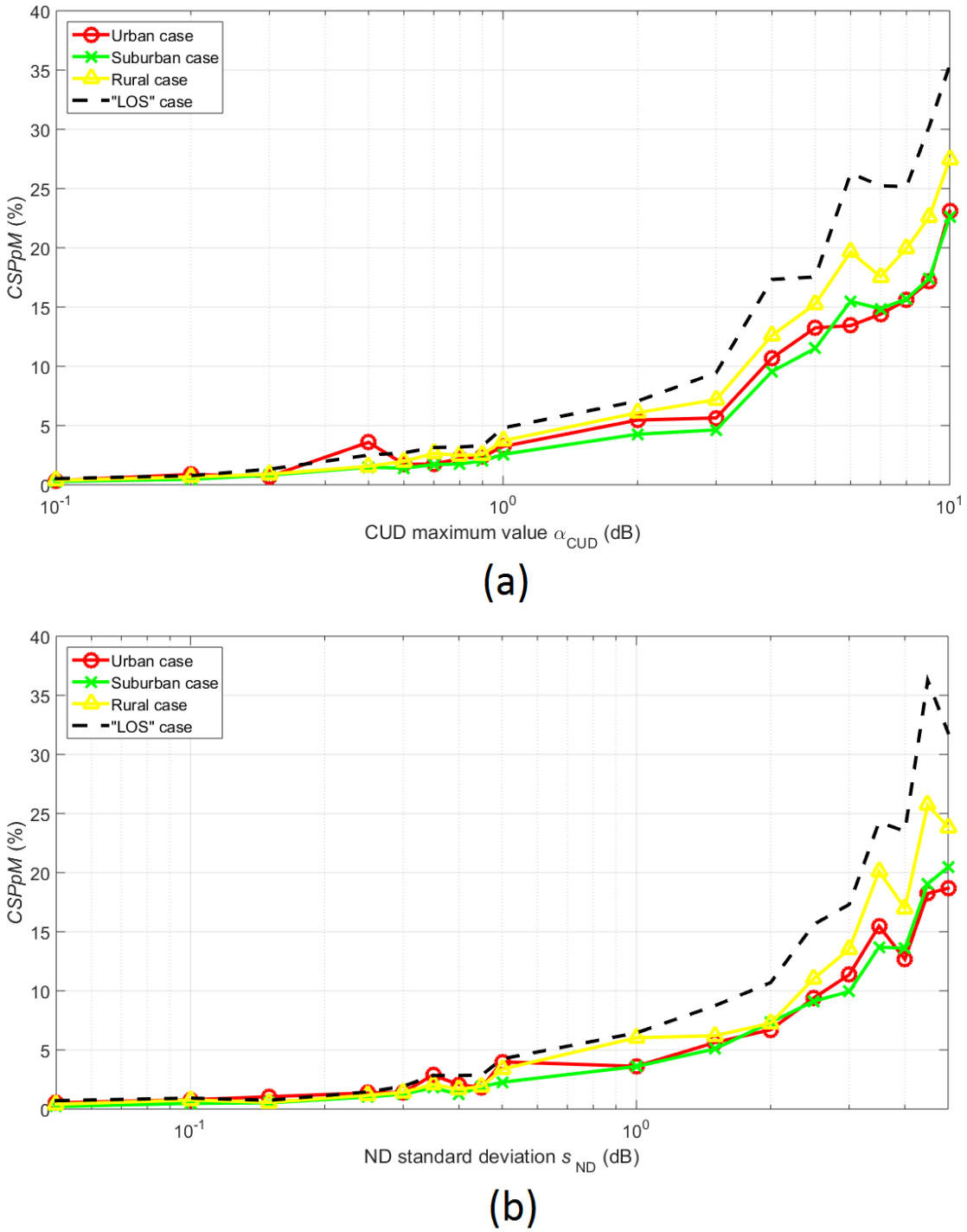

Figure 3. Same curves with Fig. 2 but for CSPpM.

4.3 Fault in Transmission Line

As already been reported in Sec.IIB, this fault subcategory deals with an interrupted transmission line across the transmission power grid. With reference to Fig. 1(b), since this fault has as a result the immediate communications failure between the transmitting and receiving end, its identification is a straightforward procedure. When such a case occurs, a warning is issued to the responsible personnel. Anyway, details

concerning the exact fault position localization are outside of the scope of this paper and this problematic case is not analyzed further.

4.4 Fault in Branch Line

This fault subcategory describes the condition where a branch line is interrupted. With reference to Fig. 1(c), let the first branch of each indicative OV HV BPL topology be broken at 100m from the branching interconnection A_1 with the transmission line. Note that the interruption of the first branch, which is treated as an open circuit in this subsection, transfers the termination from L_{b1} to $L_{b,f}$=100m, thus, converting the examined original OV HV BPL topologies into new modified ones. The modified OV HV BPL topologies are characterized by new respective OV HV BPL coupling transfer functions and measurement differences. It is expected that the multipath environment of the modified OV HV BPL topologies becomes richer than the one of the original OV HV BPL topologies due to the new shorter branch.

Even if two different measurement differences occur during the determination of the original and modified OV HV BPL coupling transfer functions, FIIM recognizes the branch line fault and warns the responsible personnel. On the basis of eq. (10), FIIM can identify branch line faults by applying $\Delta CSPpM^*$. In Fig. 4(a), CSPpM of the original urban OV HV BPL topology, CSPpM* of the modified urban OV HV BPL topology and their $\Delta CSPpM^*$ are plotted versus the CUD maximum value of the occurred measurement differences. Note that even though two different measurement difference CUDs are applied during the determination of original and modified OV HV BPL coupling transfer functions, respectively, their CUD maximum value α_{CUD} remains the same for each curve marker. This is due to the fact that the surrounding environment of either the original OV HV BPL topology or its modified version remains the same and so does the chargeable event of measurement differences. Similar curves with Fig. 4(a) are given in Figs. 4(b) and 4(c) but for the suburban and rural case, respectively.

From Figs. 4(a)-(c), it is evident that CSPM*s of all the modified OV HV BPL topologies significantly differ from the respective original CSPMs. Especially, the difference, which is expressed by the respective ΔCSPpM curves, is easily observable when measurement differences remain relatively low. As the measurement differences increase, the ΔCSpM* values decrease and so does the identification potential of branch faults.

With reference to Figs. 3(a) and 3(b), a strict ΔCSpM* threshold is proposed that comes from the equity of the examined ΔCSpM* with the CSPpM of the respective original OV HV BPL topology in order not to confuse the branch fault with the high magnitude of measurement differences. When $\Delta CSPpM^*$ is greater or equal than $\Delta CSPpM_{thr}^*$, either fault or instability surely occurs across the OV HV BPL network and a warning message must be sent to the responsible personnel. If $\Delta CSPpM^*$ ranges from approximately 2-3dB to $\Delta CSPpM_{thr}^*$ then there is significant possibility of fault across the OV HV BPL network and a preparation of the responsible personnel should be made.

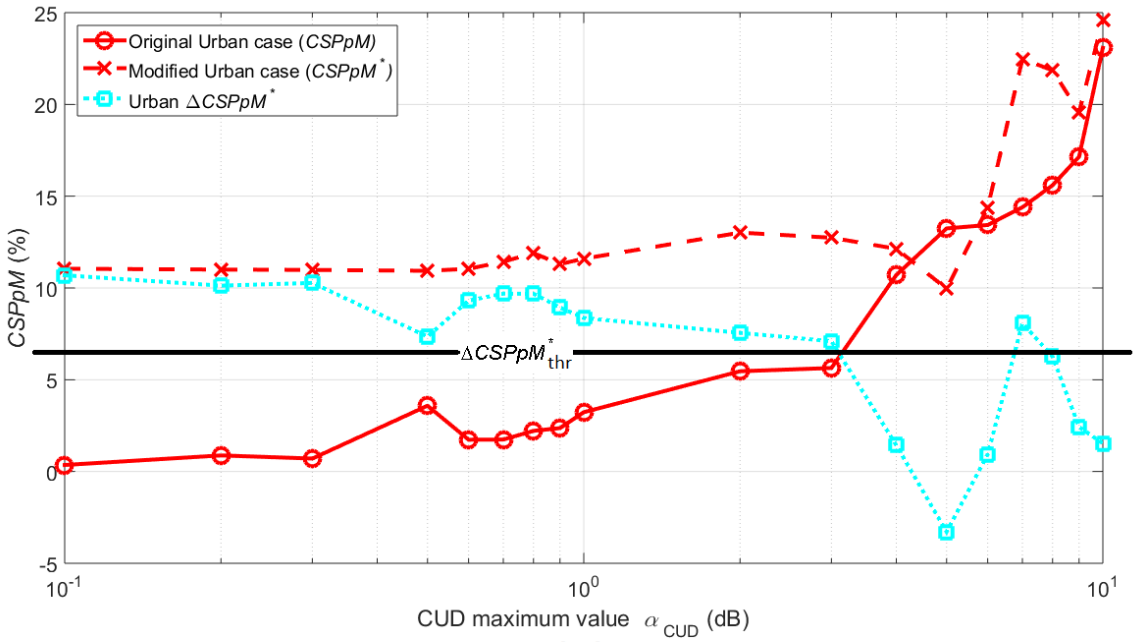
Original Urban case (CSPpM)
Modified Urban case (CSPpM*)
Urban ΔCSPpM*
ΔCSPpM*thr
CSPpM (%)
CUD maximum value α CUD (dB)
25
20
15
10
5
0
-5
10-1
100
101

(a)

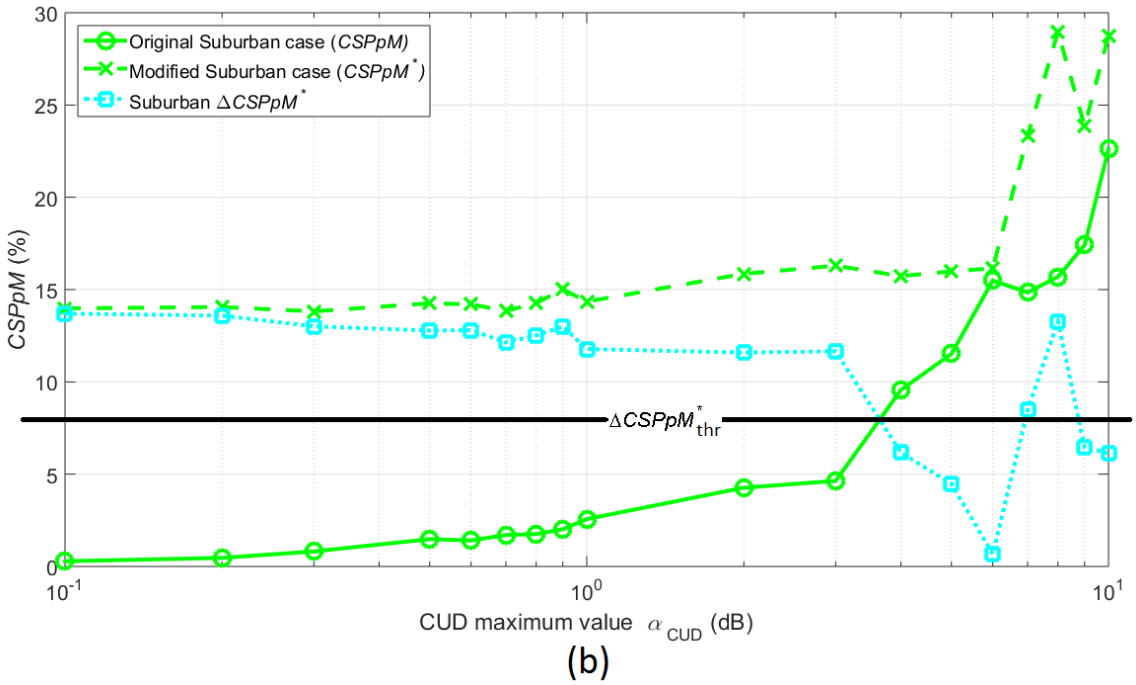

Figure 4. Fault in the first branch of the indicative OV HV BPL topologies and the behavior of CSPpM and ΔCSPpM*. (a) Urban case. (b) Suburban case. (c) Rural case.

Conversely, if $\Delta CSPpM^{*}$ is below 2-3dB then there is uncertainty concerning the presence of fault or instability across the OV HV BPL network. Not to trigger a false alert, $\Delta CSPpM_{\text{thr}}^{*}$ should receive a decent value that ranges from 6% to 9%. For example, $\Delta CSPpM_{\text{thr}}^{*}$ is equal to 6.44%, 7.97% and 8.67% for the urban, suburban and rural topology, respectively.

4.5 Instability in Branch Interconnection

This subsection examines the possibility of identifying an instability that occurs in a branch interconnection. With reference to Fig. 1(d), the interruption of the last branch at the point A_N cancels the presence of this branch, thus, converting the examined N-branch OV HV BPL topology into a (N-1)-branch OV HV BPL topology. Similarly to the faults in branch lines, the modified OV HV BPL topologies are characterized by new respective OV HV BPL coupling transfer functions and measurement differences.

Based on eq. (10), FIIM can identify branch interconnection faults by applying $\Delta CSPpM^*$. Similarly to branch line faults, in Fig. 5(a), CSPpM of the original urban OV HV BPL topology, $CSPpM^*$ of the modified urban OV HV BPL topology and their $\Delta CSPpM^*$ are plotted versus the CUD maximum value of the occurred measurement differences. Similar curves with Fig. 5(a) are given in Figs. 5(b) and 5(c) but for the suburban and rural case, respectively.

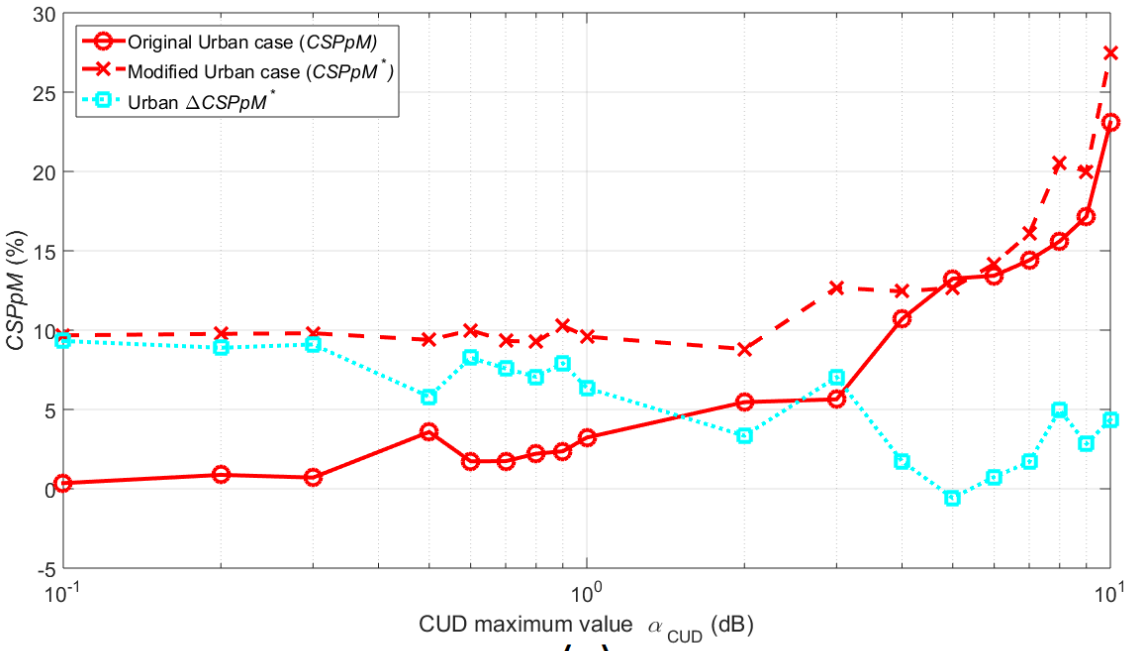
Original Urban case (CSPpM)
Modified Urban case (CSPpM*)
Urban ΔCSPpM*
CSPpM (%)
CUD maximum value α CUD (dB)

(a)

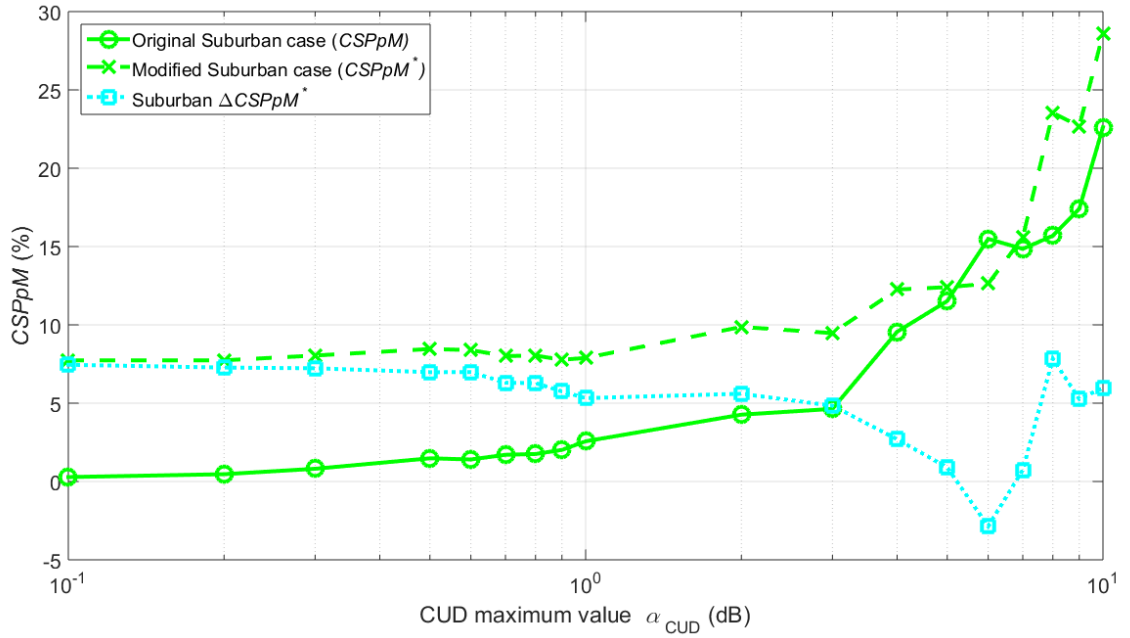
Original Suburban case (CSPpM)
Modified Suburban case (CSPpM*)
Suburban ΔCSPpM*
CSPpM (%)
CUD maximum value α CUD (dB)

(b)

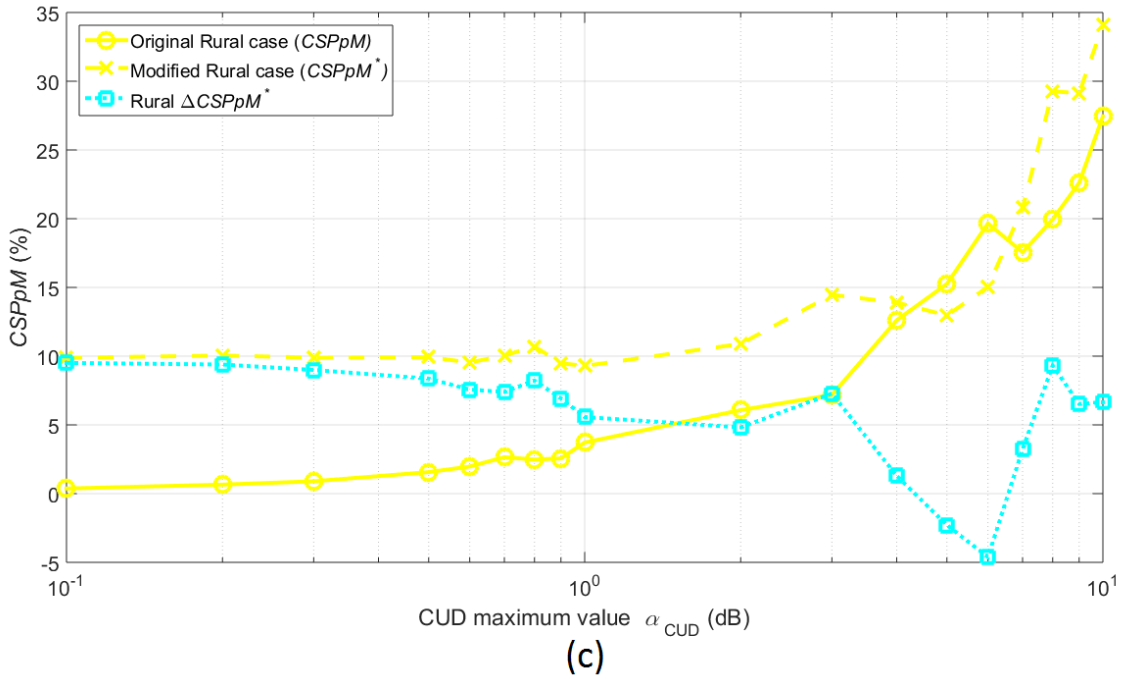

Figure 5. Instability in the last branch interconnection of the indicative OV HV BPL topologies and the behavior of CSPpM and ΔCSPpM*. (a) Urban case. (b) Suburban case. (c) Rural case.

Comparing Figs. 5(a)-(c) with the respective Figs. 4(a)-(c), $\Delta CSPpM^*$s of branch interconnection instability present lower values in comparison with the respective ones of branch line faults. This indicates that the branch interconnection instability establishes a problematic condition more difficult to be recognized in relation with the one of branch line fault. Nevertheless, $\Delta CSPpM^*$ identifies the branch interconnection instability regardless of the considered OV HV BPL topology and the applied CUD magnitude. Although the identification of the branch interconnection instability becomes more challenging when measurement differences magnitude exceeds 4dB, $\Delta CSPpM^*$ triggers the alarm in the majority of the cases since $\Delta CSPpM^*$ values exceed zero in all these cases. If a stricter decision needs to be taken then $\Delta CSPpM_{\text{thr}}^*$ ranges from 5% to 7%. The latter threshold values are lower than the ones of Sec.IVD; it is clear that the difficulty of the identification of branch interconnection instability is also reflected on $\Delta CSPpM_{\text{thr}}^*$.

4.6 Instability in Branch Terminations

This subsection examines the possibility of identifying an instability that occurs in a branch termination. Prior to proceeding to the analysis of this problematic condition, it is expected that this condition is going to be the more challenging one since FIIM needs to identify an instability that comes from a circuit anomaly at a specific piece of equipment. With reference to Fig. 1(e), let the branch termination of the first branch of each indicative OV HV BPL topology stop to act as open circuit termination. Since the branch termination fluctuates, OV HV BPL coupling transfer functions present

instabilities that resemble to measurement differences. Assuming that the modified OV HV BPL topologies present a general short circuit in their HV/MV transformers at their first branch, FIIM can identify that an instability occurs by applying $\Delta CSPpM^*$; similarly to branch line faults and branch interconnection instabilities, in Fig. 6(a), CSPpM of the original urban OV HV BPL topology, CSPpM* of the modified urban OV HV BPL topology and their $\Delta CSPpM^*$ are plotted versus the CUD maximum value of the occurred measurement differences. Similar curves with Fig. 6(a) are given in Figs. 6(b) and 6(c) but for the suburban and rural case, respectively.

Also, in Figs. 7(a)-(c), similar plots are curved with the respective Figs. 6(a)-(c) but for matched termination at the first branch (e.g., connection of a BPL unit at the HV/MV transformer).

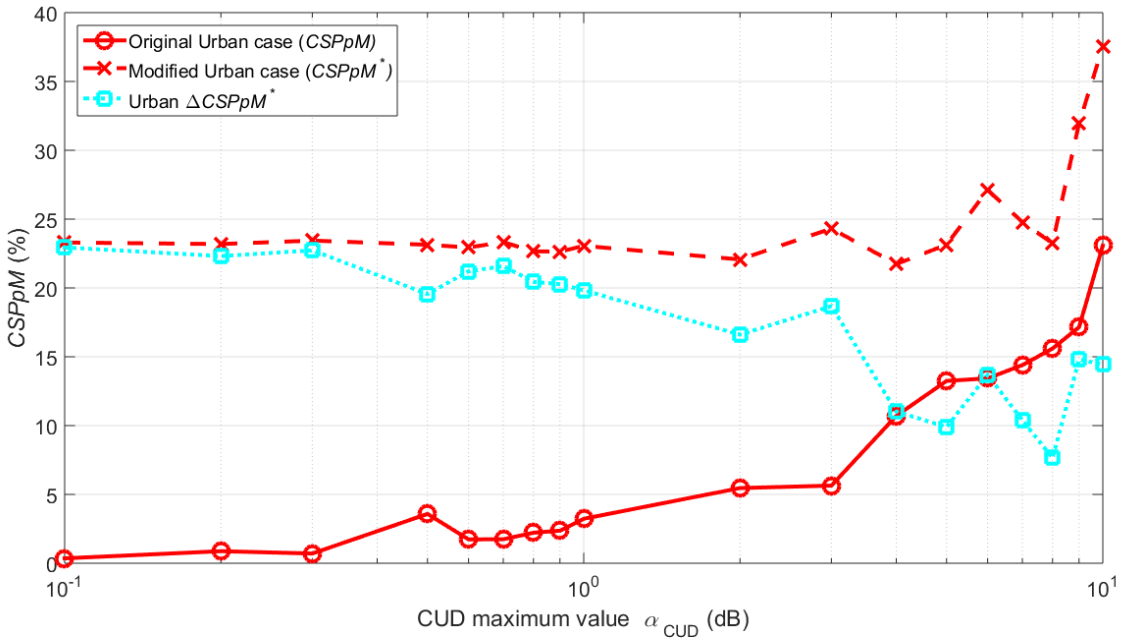
Original Urban case (CSPpM)
Modified Urban case (CSPpM*)
Urban ΔCSPpM*
CSPpM (%)
CUD maximum value α CUD (dB)

(a)

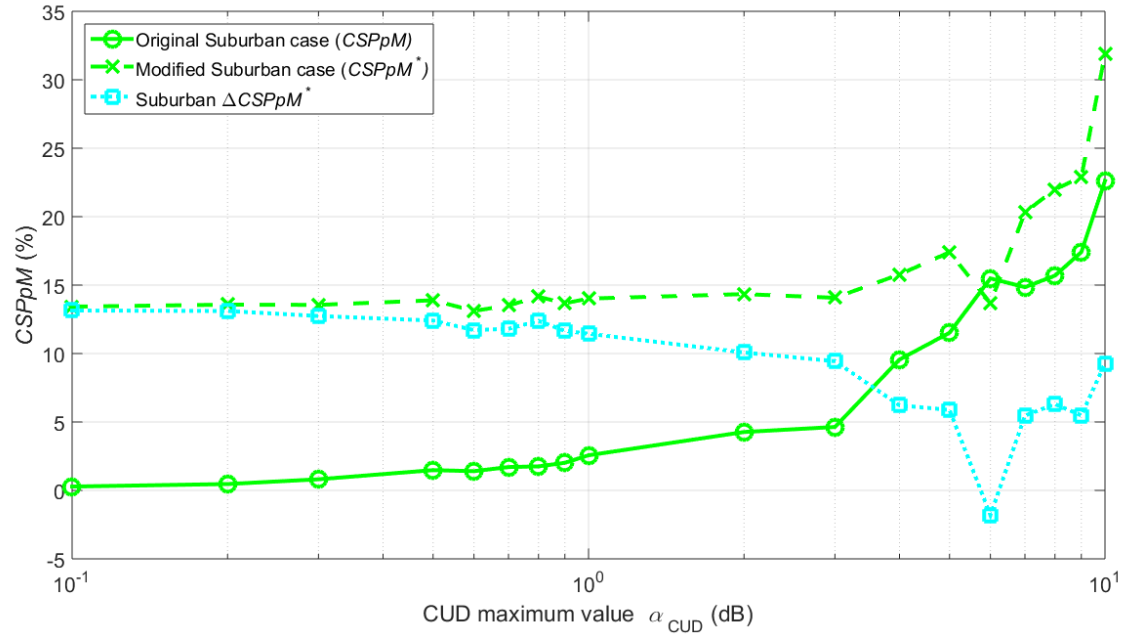
Original Suburban case (CSPpM)
Modified Suburban case (CSPpM*)
Suburban ΔCSPpM*
CSPpM (%)
CUD maximum value α CUD (dB)

(b)

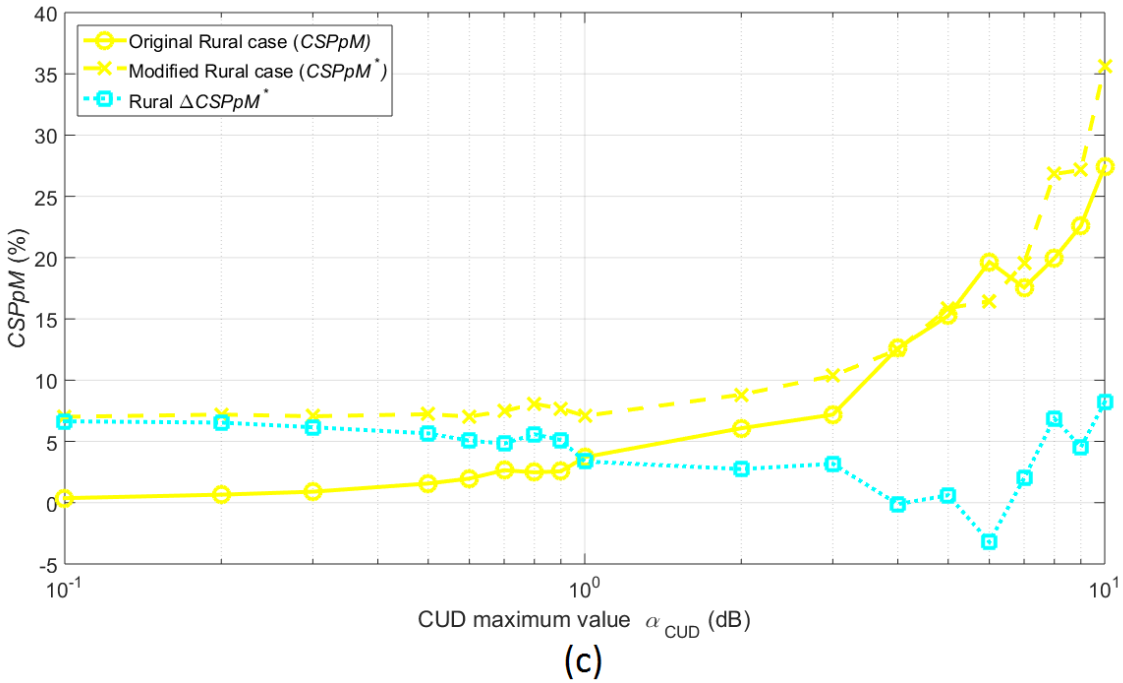

Figure 6. Termination instability (short circuit) at the first branch of the indicative OV HV BPL topologies and the behavior of CSPpM and ΔCSPpM*. (a) Urban case. (b) Suburban case. (c) Rural case.

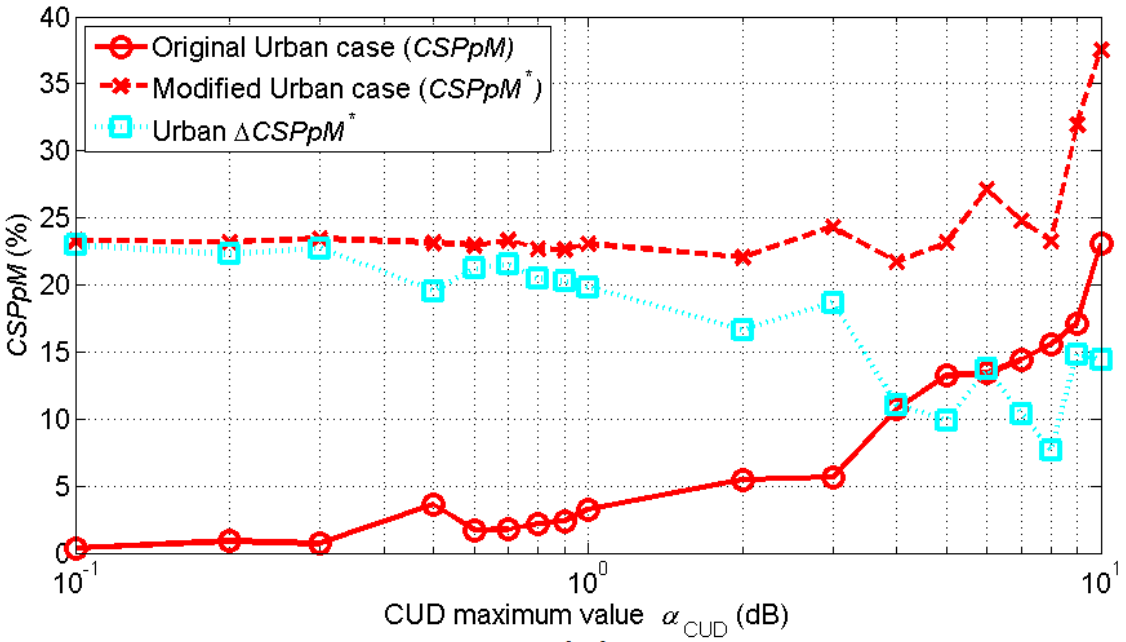
Original Urban case (CSPpM)
Modified Urban case (CSPpM*)
Urban ΔCSPpM*
CSPpM (%)
CUD maximum value α CUD (dB)

(a)

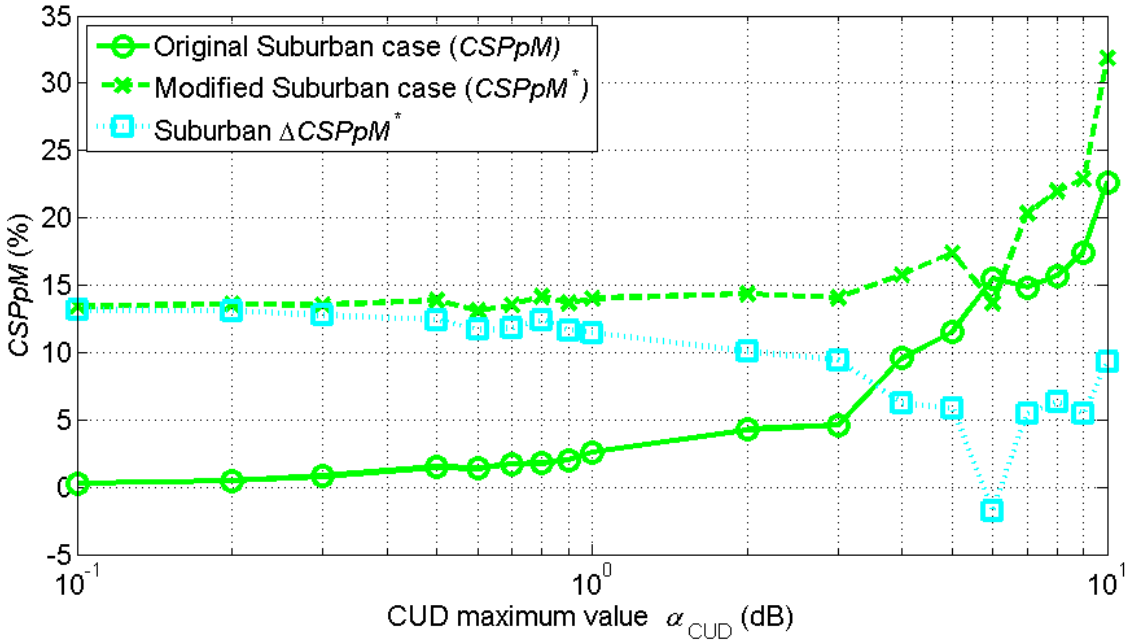
Original Suburban case (CSPpM)
Modified Suburban case (CSPpM*)
Suburban ΔCSPpM*
CSPpM (%)
CUD maximum value α CUD (dB)

(b)

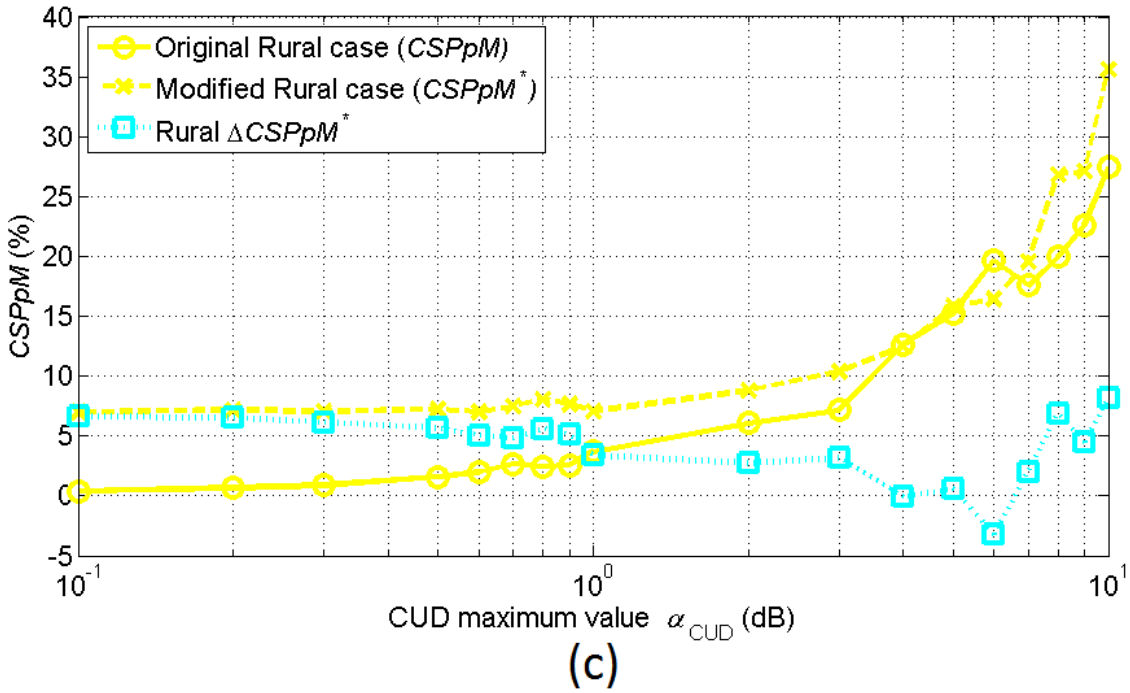

Figure 7. Same plots with Fig. 6 but for matched termination at the first branch.

From Figs. 6(a)-(c) and Figs. 7(a)-(c), FIIM can immediately identify any damage or change concerning pieces of equipment across transmission power grid. Although the termination instabilities define a rather difficult challenge, as it is seen by the lower $\Delta CSPpM_{\text{thr}}^{*}$ s in comparison with the ones of the former examined problematic conditions, FIIM can separate measurement differences from the termination instabilities. Indeed, $\Delta CSPpM^{*}$ presents positive values in the vast majority of the cases examined, even if measurement differences of 10dB are present. Also, as the length of the termination branch increases, the behavior of OV HV BPL coupling transfer function tends to the one with matched termination rendering the identification more difficult. For example, CSPpM curves of the original and modified rural case little differ each other due to this power divider behavior of long branches regardless of the type of termination –see Figs. 6(c) and Fig. 7(c)–.

4.7 Performance of Traditional FIIM

The traditional FIIM is mainly based on the observation and the experience of the responsible personnel. With reference to eq. (11), the responsible employee should recognize unusual activity between measurements of different time instances and trigger the alarm. Each time instance is assumed to be characterized by different measurement difference CUDs but of the same maximum value since the general conditions regarding the surrounding environment do not change (same as in Secs.IVC-IVF). However, the fault and instability warning of the traditional FIIM proves to be a risky venture in all the kinds of faults and instabilities. More specifically:

- *Fault in Branch Lines*: Respective figures with Figs. 4(a)-(c) are given in Figs. 8(a)-(c). More analytically, in Figs. 8(a)-(c), the PES* is plotted versus the

CUD maximum value of the occurred measurement differences for the urban, suburban and rural topology, respectively. In each figure, both the PES* of the original topology and the modified one are given when the branch line fault occurs.

- *Instability in Branch Interconnections*: Respective figures with Figs. 5(a)-(c) are given in Figs. 8(d)-(f). Note that Figs. 8(d)-(f) are the same figures with Figs. 8(a)-(c) but when the branch interconnection instability occurs.
- *Instability in Branch Terminations*: Here, two different cases are examined, as follows:
    - *Matched Termination*: Respective figures with Figs. 6(a)-(c) are presented in Figs. 8(g)-(i). Note that Figs. 8(d)-(f) are the same figures with Figs. 8(a)-(c) but when the matched termination occurs.
    - *Shor Circuit Termination*: Respective figures with Figs. 7(a)-(c) are demonstrated in Figs. 8(j)-(l). Note that Figs. 8(j)-(l) are the same figures with Figs. 8(a)-(c) but when the short circuit termination occurs.

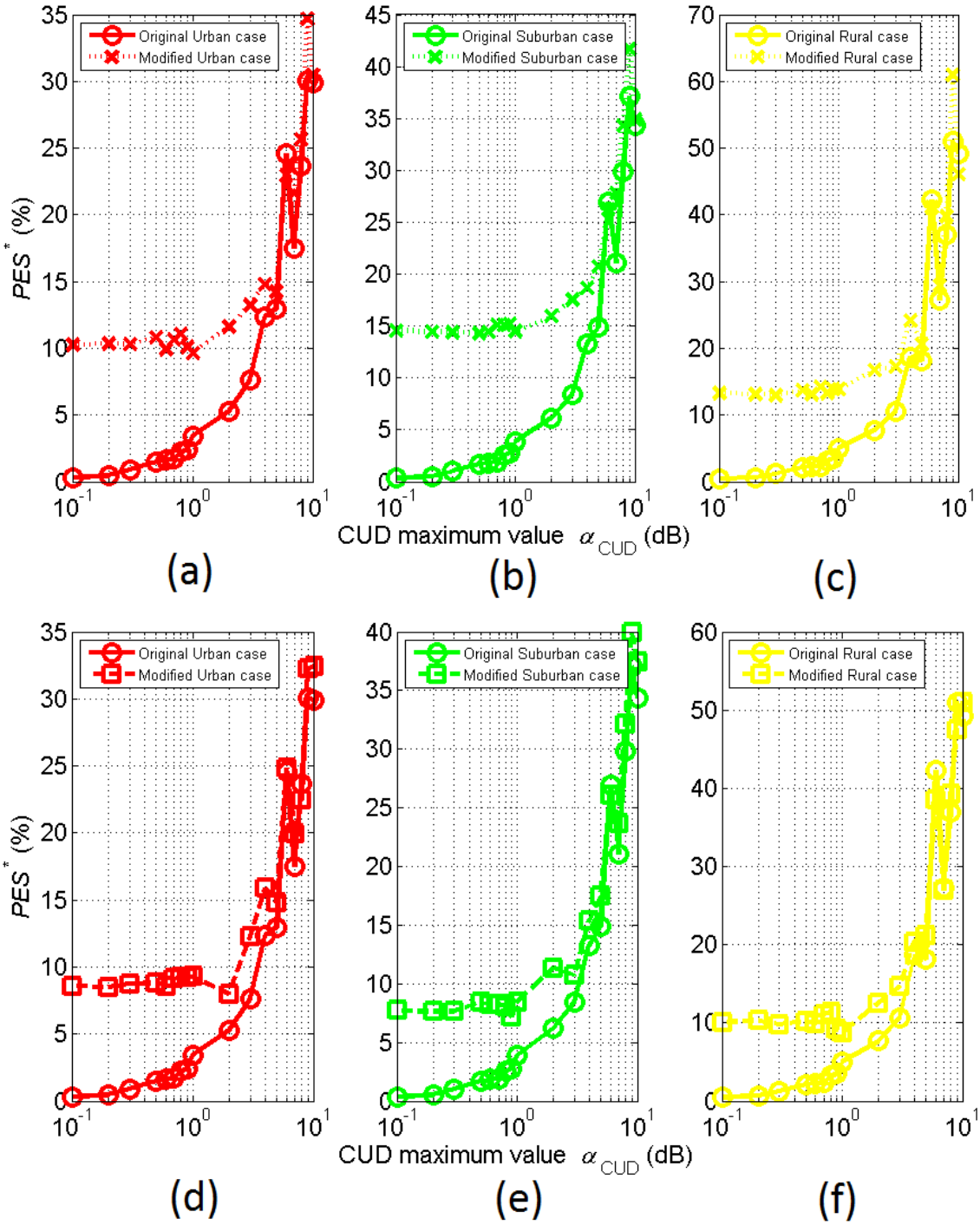
Original Urban case
Modified Urban case
Original Suburban case
Modified Suburban case
Original Rural case
Modified Rural case
PES* (%)
CUD maximum value α CUD (dB)
(a)
(b)
(c)
(d)
(e)
(f)

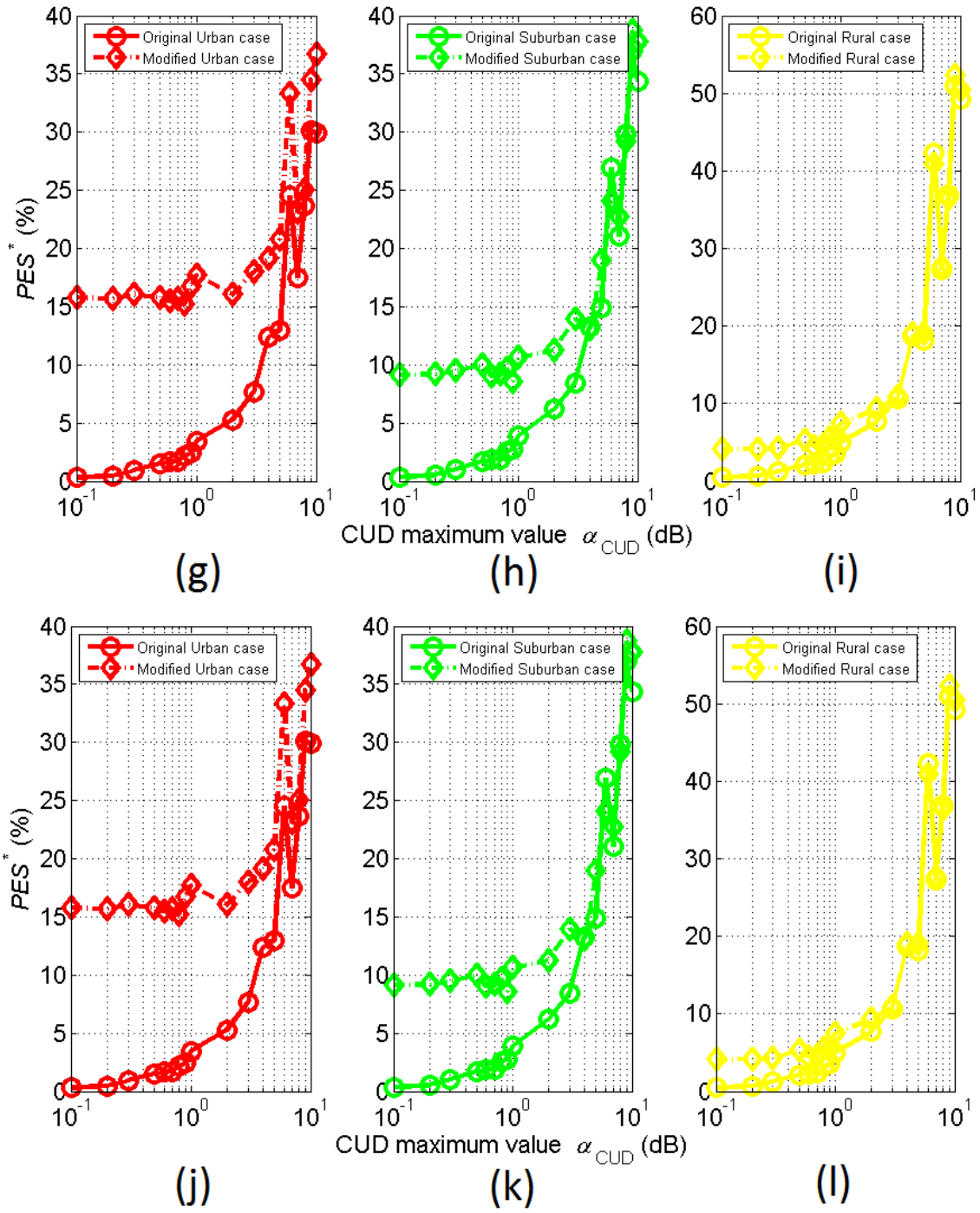

Figure 8. Traditional FIIM, faults and instabilities. (a)-(c) Branch line faults. (d)-(f) Branch interconnection instability. (g)-(i) Branch termination instability (matched termination). (j)-(l) Branch termination instability (short circuit terminations).

Comparing the performance of the proposed and traditional FIIM, it is evident that the decision regarding the various faults and instabilities that may occur across the transmission power grid is easier by applying the proposed FIIM in all the cases examined. Especially, when the measurement differences exceed 3dB, the proposed FIIM can still give a reliable identification regarding faults and instabilities despite the large

measurement differences. But the main deficiency of the traditional FIIM is its performance when faults and instabilities occur in OV HV BPL topologies of poor multipath environment (e.g., indicative rural OV HV BPL topology). In these cases, the traditional FIIM faces difficulties to identify either a fault or instability since the differences between original and modified PES* curves remain marginal even if small measurement differences are applied. In fact, PES* curves are significantly affected by the presented measurement differences in contrast with the respective ΔCSPpM* curves that are less distorted by the measurement differences due to the error filtering of the best L1PMA. Finally, if PES^*_{thr} is assumed to be equal to $CSPpM^*_{thr}$ (i.e., safe decisions are required) then traditional FIIM is treated as extremely conservative ignoring a great number of problematic conditions.

4.8 Future Research

From both papers, it is clearly indicated that either TIM or FIIM may be used as the basis for a plethora of smart grid applications concerning system protection, load and distributed generation management, distribution automations and diagnostic monitoring [52]. More analitically, among the following research steps, the combined operation of TIM and FIIM is going to focus on: (i) fault recognition and location; (ii) VAR control; (iii) isolation of faults on single phases; (iv) predictive maintenance; and (v) EMI and noise analysis.

To implement the aforementioned research goals, some structural changes should be made either in TIM or in FIIM procedure. As the TIM is concerned, the OV HV BPL topology database should be enriched so that higher accuracy is achieved (i.e., lower values for the length spacing, higher values for the maximum branch length and a variety of branch terminations) and more multi-branch OV HV BPL topologies are inserted. This implies that significant work should be done in the field of the optimization of the database (i.e., faster algorithms during the database creation, insertion and update). As the FIIM is concerned, CSPpM curves should be further analyzed in order to become identity metrics for the OV HV BPL topologies and ΔCSPpM* curves should be further investigated in order to become fault identities for various faults and instabilities that may occur across the transmission power grid. Finally, to become real-time application, significant optimization efforts should be concentrated to the minimization of FIIM computations and the reduction of today's overall execution times of FIIM for the various fault and instability conditions.

5. Conclusions

In this companion paper, the proposed TIM of [1] has extended to FIIM that deals with the fault and instability identification across transmission power grids. FIIM consists of: (i) the hybrid method; (ii) the best L1PMA; (iii) TIM; and (iv) CSPpM and ΔCSPpM* that serve as fault identification metrics.

As the assessment of the FIIM is concerned, FIIM has easily achieved to identify faults in branch lines, instabilities in branch interconnections and instabilities in branch terminations of various kinds during the real-time operation of indicative OV HV BPL topologies. Actually, FIIM have identified the faults and instabilities in all the cases examined even though measurement differences up to 10dB have been considered.

Exploiting the virtues of the emerging intelligent energy systems, both TIM and FIIM can be an invaluable tool during the surveillance and monitoring of transmission and distribution power grid supporting a myriad of smart grid applications.

Conflicts of Interest

The author declares that there is no conflict of interests regarding the publication of this paper.

References

[1] A. G. Lazaropoulos, "Measurement Differences, Faults and Instabilities in Intelligent Energy Systems – Part 1: Identification of Overhead High-Voltage Broadband over Power Lines Network Topologies by Applying Topology Identification Methodology (TIM)," *Trends in Renewable Energy*, vol. 2, no. 3, pp. 85-112, 2016. DOI: 10.17737/tre.2016.2.3.0026

[2] A. Milioudis, G. T. Andreou, and D. P. Labridis, "Detection and location of high impedance faults in multiconductor overhead distribution lines using power line communication devices," *IEEE Trans. on Smart Grid*, vol. 6, no. 2, pp. 894-902, 2015.

[3] T. A. Papadopoulos, A. I. Chrysochos, E. O. Kontis, and G. K. Papagiannis, "Ringdown Analysis of Power Systems Using Vector Fitting," *Electric Power Systems Research*, vol. 141, pp. 100-103, 2016.

[4] A. Milioudis, G. Andreou, and D. Labridis, "Optimum transmitted power spectral distribution for broadband power line communication systems considering electromagnetic emissions," *Elsevier Electric Power Systems Research*, in press, 2016.

[5] S. S. Pappas, L. Ekonomou, D. C. Karamousantas, G. E. Chatzarakis, S. K. Katsikas, and P. Liatsis, "Electricity Demand Loads Modeling Using AutoRegressive Moving Average (ARMA) Models," Energy, vol. 33, no. 9, pp. 1353-1360, 2008. DOI: 10.1016/j.energy.2008.05.008

[6] R. Lee and R. H. Osborn, "A microcomputer based data acquisition system for high impedance fault analysis," *IEEE Power Eng. Rev.*, vol. PER-5, no. 10, p. 35, Oct. 1985.

[7] S. Ebron, D. Lubkeman, and M. White, "A neural network approach to the detection of incipient faults on power distribution feeders," *IEEE Trans. Power Del.*, vol. 5, no. 2, pp. 905–914, Apr. 1990.

[8] J.-H. Ko, J.-C. Shim, C.-W. Ryu, C.-G. Park, and W.-Y. Yim, Detection of high impedance faults using neural nets and chaotic degree," in *Proc. 1998 Int. Conf. Energy Manage. Power Del. (EMPD)*, vol. 2. Singapore, pp. 399–404.

[9] F. Jota and P. R. S. Jota, "High-impedance fault identification using a fuzzy reasoning system," *IEE Proc. Gener. Transmiss. Distrib.*, vol. 145, no. 6, pp. 656–661, Nov. 1998.

[10] Y. Sheng and S. Rovnyak, "Decision tree-based methodology for high impedance fault detection," *IEEE Trans. Power Del.*, vol. 19, no. 2, pp. 533–536, Apr. 2004.

[11] D. C. T. Wai and X. Yibin, "A novel technique for high impedance fault identification," *IEEE Trans. Power Del.*, vol. 13, no. 3, pp. 738–744, Jul. 1998.

[12] I. Zamora, A. Mazon, K. J. Sagastabeitia, and J. Zamora, "New method for detecting low current faults in electrical distribution systems," *IEEE Trans. Power Del.*, vol. 22, no. 4, pp. 2072–2079, Oct. 2007.

[13] J. Zamora, I. Zamora, A. Mazon, and K. J. Sagastabeitia, "Optimal frequency value to detect low current faults superposing voltage tones," *IEEE Trans. Power Del.*, vol. 23, no. 4, pp. 1773–1779, Oct. 2008.

[14] M. Michalik, W. Rebizant, M. Lukowicz, S.-J. Lee, and S.-H. Kang, "High-impedance fault detection in distribution networks with use of wavelet-based algorithm," *IEEE Trans. Power Del.*, vol. 21, no. 4, pp. 1793–1802, Oct. 2006.

[15] M. Michalik, M. Lukowicz, W. Rebizant, S.-J. Lee, and S.-H. Kang, "Verification of the wavelet-based HIF detecting algorithm performance in solidly grounded MV networks," *IEEE Trans. Power Del.*, vol. 22, no. 4, pp. 2057–2064, Oct. 2007.

[16] B. Aucoin and B. Russell, "Distribution high impedance fault detection utilizing high frequency current components," *IEEE Trans. Power App. Syst.*, vol. PAS-101, no. 6, pp. 1596–1606, Jun. 1982.

[17] A. N. Milioudis, G. T. Andreou, and D. P. Labridis, "Enhanced Protection Scheme for Smart Grids Using Power Line Communications Techniques—Part II: Location of High Impedance Fault Position," *IEEE Trans. on Smart Grid*, no. 3, vol. 4, pp. 1631-1640, 2012.

[18] A. Milioudis, G. Andreou, and D. Labridis, "High impedance fault detection using power line communication techniques," in *Proc. 2010 45th Int. Univ. Power Eng. Conf. (UPEC)*, Cardiff, U.K., pp. 1–6.

[19] A. Milioudis, G. Andreou, and D. Labridis, "High impedance fault evaluation using narrowband power line communication techniques," in *Proc. 2011 IEEE Trondheim PowerTech*, Trondheim, Norway, pp. 1–6.

[20] A. Milioudis, G. Andreou, and D. Labridis, "Enhanced protection scheme for smart grids using power line communications techniques—Part I: Detection of high impedance fault occurrence," *IEEE Trans. Smart Grid*, vol. 3, no. 4, pp. 1621–1630, Dec. 2012.

[21] A. I. Chrysochos, T. A. Papadopoulos, A. ElSamadouny, G. K. Papagiannis, and N. Al-Dhahir, "Optimized MIMO-OFDM design for narrowband-PLC applications in medium-voltage smart distribution grids," *Electric Power Systems Research*, vol. 140, pp. 253–262, 2016. DOI: 10.1016/j.epsr.2016.06.017

[22] A. G. Lazaropoulos, "Factors Influencing Broadband Transmission Characteristics of Underground Low-Voltage Distribution Networks," *IET Commun.*, vol. 6, no. 17, pp. 2886-2893, Nov. 2012.

[23] A. G. Lazaropoulos and P. G. Cottis, "Transmission characteristics of overhead medium voltage power line communication channels," *IEEE Trans. Power Del.*, vol. 24, no. 3, pp. 1164-1173, Jul. 2009.

[24] A. G. Lazaropoulos and P. G. Cottis, "Capacity of overhead medium voltage power line communication channels," *IEEE Trans. Power Del.*, vol. 25, no. 2, pp. 723-733, Apr. 2010.

[25] A. G. Lazaropoulos and P. G. Cottis, "Broadband transmission via underground medium-voltage power lines-Part I: transmission characteristics," *IEEE Trans. Power Del.*, vol. 25, no. 4, pp. 2414-2424, Oct. 2010.

[26] A. G. Lazaropoulos and P. G. Cottis, "Broadband transmission via underground medium-voltage power lines-Part II: capacity," *IEEE Trans. Power Del.*, vol. 25, no. 4, pp. 2425-2434, Oct. 2010.

[27] A. G. Lazaropoulos, "Broadband transmission characteristics of overhead high-voltage power line communication channels," *Progress in Electromagnetics Research B*, vol. 36, pp. 373-398, 2012. [Online]. Available: http://www.jpier.org/PIERB/pierb36/19.11091408.pdf

[28] A. G. Lazaropoulos, "Towards broadband over power lines systems integration: Transmission characteristics of underground low-voltage distribution power lines,"

Progress in Electromagnetics Research B, 39, pp. 89-114, 2012. [Online]. Available: http://www.jpier.org/PIERB/pierb39/05.12012409.pdf

[29] A. G. Lazaropoulos, "Broadband transmission and statistical performance properties of overhead high-voltage transmission networks," *Hindawi Journal of Computer Networks and Commun.*, 2012, article ID 875632, 2012. [Online]. Available: http://www.hindawi.com/journals/jcnc/aip/875632/

[30] A. G. Lazaropoulos, "Towards modal integration of overhead and underground low-voltage and medium-voltage power line communication channels in the smart grid landscape: model expansion, broadband signal transmission characteristics, and statistical performance metrics (Invited Paper)," *ISRN Signal Processing*, in press, [Online]. Available: http://www.isrn.com/journals/sp/aip/121628/

[31] A. G. Lazaropoulos, "Review and Progress towards the Common Broadband Management of High-Voltage Transmission Grids: Model Expansion and Comparative Modal Analysis," *ISRN Electronics*, vol. 2012, Article ID 935286, pp. 1-18, 2012. [Online]. Available: http://www.hindawi.com/isrn/electronics/2012/935286/

[32] A. G. Lazaropoulos, "Review and Progress towards the Capacity Boost of Overhead and Underground Medium-Voltage and Low-Voltage Broadband over Power Lines Networks: Cooperative Communications through Two- and Three-Hop Repeater Systems," *ISRN Electronics*, vol. 2013, Article ID 472190, pp. 1-19, 2013. [Online]. Available: http://www.hindawi.com/isrn/electronics/aip/472190/

[33] A. G. Lazaropoulos, "Green Overhead and Underground Multiple-Input Multiple-Output Medium Voltage Broadband over Power Lines Networks: Energy-Efficient Power Control," *Springer Journal of Global Optimization*, vol. 2012 / Print ISSN 0925-5001, pp. 1-28, Oct. 2012.

[34] P. Amirshahi and M. Kavehrad, "High-frequency characteristics of overhead multiconductor power lines for broadband communications," *IEEE J. Sel. Areas Commun.*, vol. 24, no. 7, pp. 1292-1303, Jul. 2006.

[35] T. Sartenaer, "Multiuser communications over frequency selective wired channels and applications to the powerline access network" Ph.D. dissertation, Univ. Catholique Louvain, Louvain-la-Neuve, Belgium, Sep. 2004.

[36] T. Calliacoudas and F. Issa, ""Multiconductor transmission lines and cables solver," An efficient simulation tool for plc channel networks development," presented at the *IEEE Int. Conf. Power Line Communications and Its Applications*, Athens, Greece, Mar. 2002.

[37] A. G. Lazaropoulos, "Best L1 Piecewise Monotonic Data Approximation in Overhead and Underground Medium-Voltage and Low-Voltage Broadband over Power Lines Networks: Theoretical and Practical Transfer Function Determination," *Hindawi Journal of Computational Engineering*, vol. 2016, Article ID 6762390, 24 pages, 2016. doi: 10.1155/2016/6762390.

[38] I. C. Demetriou and M. J. D. Powell, "Least squares smoothing of univariate data to achieve piecewise monotonicity," *IMA J. of Numerical Analysis*, vol. 11, pp. 411-432, 1991.

[39] I. C. Demetriou and V. Koutoulidis"On Signal Restoration by Piecewise Monotonic Approximation", in Lecture Notes in Engineering and Computer Science: *Proceedings of The World Congress on Engineering 2013*,London, U.K., Jul. 2013, pp. 268-273.

[40] I. C. Demetriou, "An application of best *L*1 piecewise monotonic data approximation to signal restoration," *IAENG International Journal of Applied Mathematics*, vol. 53, no. 4, pp. 226-232, 2013.
[41] I. C. Demetriou, "L1PMA: A Fortran 77 Package for Best L1 Piecewise Monotonic Data Smoothing," *Computer Physics Communications*, vol. 151, no. 1, pp. 315-338, 2003.
[42] I. C. Demetriou, "Data Smoothing by Piecewise Monotonic Divided Differences," *Ph.D. Dissertation*, Department of Applied Mathematics and Theoretical Physics, University of Cambridge, Cambridge, 1985.
[43] I. C. Demetriou, "Best L1 Piecewise Monotonic Data Modelling,"*Int. Trans. Opl Res.*, vol. 1, no. 1, pp. 85-94,1994.
[44] I.C. Demetriou, "L1PMA: a Fortran 77 package for best L1 piecewise monotonic data smoothing," 2003 http://cpc.cs.qub.ac.uk/summaries/ADRF
[45] T. Sartenaer and P. Delogne, "Deterministic modelling of the (Shielded) outdoor powerline channel based on the multiconductor transmission line equations," *IEEE J. Sel. Areas Commun.*, vol. 24, no. 7, pp. 1277-1291, Jul. 2006.
[46] OPERA1, D5: Pathloss as a function of frequency, distance and network topology for various LV and MV European powerline networks. IST Integrated Project No 507667, Apr. 2005.
[47] P. Amirshahi, "Broadband access and home networking through powerline networks" Ph.D. dissertation, Pennsylvania State Univ., University Park, PA, May 2006. [Online]. Available: http://etda.libraries.psu.edu/theses/approved/WorldWideIndex/ETD-1205/index.html
[48] OPERA1, D44: Report presenting the architecture of plc system, the electricity network topologies, the operating modes and the equipment over which PLC access system will be installed, IST Integr. Project No 507667, Dec. 2005.
[49] T. Banwell and S. Galli, "A novel approach to accurate modeling of the indoor power line channel—Part I: Circuit analysis and companion model," *IEEE Trans. Power Del.*, vol. 20, no. 2, pp. 655-663, Apr. 2005.
[50] S. Galli and T. Banwell, "A novel approach to accurate modeling of the indoor power line channel — Part II: Transfer function and channel properties," *IEEE Trans. Power Del.*, vol. 20, no. 3, pp. 1869-1878, Jul. 2005.
[51] S. Galli and T. Banwell, "A deterministic frequency-domain model for the indoor power line transfer function," *IEEE J. Sel. Areas Commun.*, vol. 24, no. 7, pp. 1304-1316, Jul. 2006.
[52] A. G. Lazaropoulos, A. M. Sarafi, and P. G. Cottis, "The emerging smart grid — A pilot MV/BPL network installed at Lavrion, Greece," in *Proc. Workshop on Applications for Powerline Communications WSPLC 2008*, Thessaloniki, Greece, Oct. 2008. [Online]. Available: http://newton.ee.auth.gr/WSPLC08/Abstracts%5CSG_3.pdf

CALL FOR PAPERS

Trends in Renewable Energy

ISSN Print: 2376-2136 ISSN online: 2376-2144

http://futureenergysp.com/index.php/tre/

Trends in Renewable Energy (TRE) is an open accessed, peer-reviewed semi-annual journal publishing reviews and research papers in the field of renewable energy technology and science. The aim of this journal is to provide a communication platform that is run exclusively by scientists. This journal publishes original papers including but not limited to the following fields:

- ✧ Renewable energy technologies
- ✧ Catalysis for energy generation, Green chemistry, Green energy
- ✧ Bioenergy: Biofuel, Biomass, Biorefinery, Bioprocessing, Feedstock utilization, Biological waste treatment,
- ✧ Energy issues: Energy conservation, Energy delivery, Energy resources, Energy storage, Energy transformation, Smart Grid
- ✧ Environmental issues: Environmental impacts, Pollution
- ✧ Bioproducts
- ✧ Policy, etc.

We publish the following article types: peer-reviewed reviews, mini-reviews, technical notes, short-form research papers, and original research papers.

The article processing charge (APC), also known as a publication fee, is fully waived for the Trends in Renewable Energy.

Call for Editorial Board Members

We are seeking scholars active in a field of renewable energy interested in serving as volunteer Editorial Board Members.

Qualifications

Ph.D. degree in related areas, or Master's degree with a minimum of 5 years of experience. All members must have a strong record of publications or other proofs to show activities in the energy related field.

If you are interested in serving on the editorial board, please email CV to editor@futureenergysp.com.